Journal of
*Marine Science and Engineering*

MDPI

*Article*

# Investigation on hydrodynamic characteristics, wave-current interaction, and sensitivity analysis of submarine hoses attached to a CALM buoy

**Chiemela Victor Amaechi [1,2,*], Facheng Wang [3,*], and Jianqiao Ye [1,*]**

[1] Department of Engineering, Lancaster University, Lancaster, LA1 4YR, UK
[2] Standards Organisation of Nigeria (SON), 52 Lome Crescent, Wuse Zone 7, Abuja, 900287, Nigeria.
[3] Department of Civil Engineering, Tsinghua University, Beijing, 100084, China
* Correspondence: c.amaechi@lancaster.ac.uk or chiemelavic@gmail.com (C.V.A.); wangfacheng@tsinghua.edu.cn (F.W.); j.ye2@lancaster.ac.uk (J.Y).

**Citation:** Amaechi, C.V.; Wang, F.; Hou X.; Ye, J. Investigation on hydrodynamic characteristics, wave-current interaction and sensitivity analysis of submarine hoses attached to a CALM buoy. *J. Mar. Sci. Eng.* **2021**, *9*, x. https://doi.org/10.3390/xxxxx

Academic Editor: Firstname Last-name

Received: date
Accepted: date
Published: date

**Publisher's Note:** MDPI stays neutral with regard to jurisdictional claims in published maps and institutional affiliations.



**Abstract:** There is an increase in the utilisation of the floating offshore structure (FOS) called Catenary Anchor Leg Mooring (CALM) buoys and the attached marine hoses due to the increasing demand for oil and gas products. These hoses are flexible and easier to use but have a short service life of about 25 years. They are adaptable in ocean locations of shallow, intermediate, and deep waters. In this research, the numerical model was developed using a coupling method modelled by utilising ANSYS AQWA and Orcaflex dynamic models of the CALM buoy hoses. Two cases were comparatively studied: Lazy-S and Chinese-lantern configurations, under ocean waves and current. Comparisons were also made between coupled and uncoupled models. This research presents the hydrodynamic characteristics with sensitivity analysis on the influence of waves, current attack angle, soil gradient, soil stiffness, and environmental conditions that influence the performance of marine hoses. The study comparatively looked at the configurations from dynamic amplification factors (DAF) on marine hoses. The results show that marine hoses can be configured easily to suit the designer's need, seabed soil type, seabed topography, and the profiles are useful for manufacturers. The sensitivity analysis also shows the effect of hose parameters on its hydrodynamic behaviour from wave-current interaction (WCI).

**Keywords:** Ocean Wave Hydrodynamics; Catenary Anchor Leg Mooring (CALM) buoy; Lazy-S Configuration; Chinese-Lantern configuration; Marine Bonded Hose; Sensitivity; submarine hose; floating hose; hydrodynamics; ocean engineering; bonded marine hoses; marine riser; ocean waves; floating offshore platform (fos); wave-current interaction (WCI).

## 1. Introduction

Recently, applications of bonded flexible risers, unbonded flexible risers, composite risers, and marine hoses have increased in the marine industry [1-9]. This is due to the need for more flexible offshore platforms and lighter sustainable materials [10-17]. These are utilised for discharging, loading, and ocean monitoring. Marine bonded hoses are light conduit structures for fluid transportation from an offshore platform to a tanker/FPSO/FSO [18-25]. Since advances into deep water explorations have increased the need for more sustainable and cost-efficient platforms, these marine structures have received increased attention for application in offshore loading and offloading operations. Thus, the need for Catenary Anchor Leg Mooring (CALM) buoys and other flexible structures. Larger floating offshore structures (FOS) like Paired Column Semisubmersibles (PCSemis), FPSOs, and Very Large Floating Structures (VLFS) do not have much such flexibility [26-33]. They also require a larger area on the sea for installation and operation, unlike the CALM buoy hose systems. The classification of marine hoses includes submarine hoses, reeling hoses, and floating hoses [34-41] based on different material and hose design configurations [42-49]. These marine bonded hoses each have different pressure ratings, such as 9 bar, 19 bar, and 21 bar ratings. However, these hoses have short service life of about 25 years, thus the need for more sensitivity studies on the load response behaviour of marine bonded hoses, as proposed herein. Secondly, the effect of wave forces on buoys can impact the floater's motion because of the sheer narrow water plane area. Thus, wave-current interaction (WCI) is pertinent for hydrodynamic sensitivity studies on the buoy-hose system. A typical CALM buoy with turret-design is shown in Figure 1, located at Apache Stag Field, Australia, during installation [49].

*Figure 1 CALM Turret buoy at Apache Stag Field, Australia, Buoy during installation (Courtesy: Bluewater [49])*

Studies on WCI, including the effect of current velocity, have been conducted both on different climatic conditions [50-54] and various FOS like semisubmersible platforms [55,56], floating wind turbines [57,58], among others. However, the literature search shows no literature has presented the effect of current velocity on the wave forces acting on the CALM buoy motion. Waves, wind, and currents are important components of the environmental loads on FOS like buoys [61-65]. To compute wave forces on offshore structures, wave theories such as the linear wave theories -Stokes wave theory and Airy wave theory, are utilized [66,67]. Conversely, over the past decades, wave loadings on FOS have been calculated using linear theory [68,69], second-order wave forces [70-75], and Morison's equation [76-78]. However, due to different constraints, Morison's equation has been modified [76,77]. Morison's equation is used to determine the inertial and drag components of the FOS's body, as well as the body's inertial and drag components [78]. However, Morison's equation is insufficient for evaluating wave forces on offshore constructions since it ignores wave diffraction. Thus, wave theories that consider diffraction are widely employed. There are limitations to the Morison's equation since it was proposed by Morison for piles but applicable in various offshore design formulations [78-84]. Many studies on cylinders and piles have led to a better understanding of the hydrodynamics of cylindrical bodies like cylindrical FPSOs and cylindrical CALM buoys. MARIN has also conducted some model tests on CALM buoy motion with recommendations for damping in pitch, heave and roll motions [85,86]. Potential theory has also made it easier to estimate the flow around spheres, buoys, and cylinders. The potential theory does define the fluid domain and wave forces surrounding the subsea marine hose as an offshore structure [87-89]. Bhatta & Rahman [90] used differential equations and Lighthill's [90,91] perturbation approach to produce a subsea hose segment's boundary conditions, forces, and moments, by utilising radiation / diffraction theory. Some reports have found nonlinearities in materials have also been observed in hose dynamics, and presented with dynamical equations formulated for marine hoses [92-94]. Other mathematical models based on the potential theory on CALM buoy hydrodynamics have also been presented [95-100]. The challenges of the incident, scattered, and diffraction wave potentials have long been debated in the offshore industry. These successfully approached wave theories have been developed to solve some of these issues. Wave forces can generate stresses due to material complexities, leading to excessive motion predictions, system failures, and material breakdowns [101-103]. They could produce substantial deformations, bending, and torsional forces in marine hoses. As a result, hydrodynamic sensitivity analysis of the floating structure's motion behaviour is required. Validated studies avow that hydrodynamic loads are used to assay the strength of various FOS, hull designs, and components utilized in fluid transfer like composite marine risers and offshore hoses [104-108]. However, wave action has an impact on the motion and strength of CALM buoy hose systems. Wave loads are also considered during hose connection operations, hose riser deployments, and hoseline/pipeline installations [109,110]. Based on hydrodynamic sensitivity studies, different sensitivity studies have been conducted for marine hoses and marine risers [111-113]. Pecher et al. [113] conducted sensitivity and comparative studies on CALM and SALM mooring for Wave Energy Converters (WECs). Sun & Wang [114] presented a sensitivity analysis on Lazy-Wave Flexible Riser modelled in ABAQUS to investigate the parameters of the buoyancy modules on the riser. In that study, the outer diameter and position of the buoyancy module were opined as high-sensitivity variables. In addition, the outside diameter had a significant impact on the riser's section moment, whereas the placement had an impact on both section force and section moment. The impact of length on the overall performance of the riser was minimal, according to the research. Amaechi et al. [115] presented a sensitivity study by comparatively looking at the parametric configurations of marine hoses, using a uniquely coupled model developed using Orcaflex’s line elements. Bidgoli et al. [116] presented a sensitivity analysis of different deepwater riser configurations modelled with Conventional Mooring Systems (CMS). Their study chose three distinct forms of the more commonly utilized deep water risers and combined them with the mooring systems, yielding six alternative case studies modelled in the OrcaFlex program. Axelsson & Skjerve [117] investigated the sensitivity of bending and radial gaps on the collapse analyses of flexible riser carcass developed in LS-Dyna and MARC. Sensitivities on straight and curved pipe sections, axially preloaded carcass, carcass ovality, the radial gap between carcass and pressure sheets, and pressure increase velocity were all part of the investigation. On the tension parameter, Tang et al. [118] investigated the influence of bending, displacement, and tension on marine drilling risers in finite element modelling (FEM) using ABAQUS. Whereas Zhang et al. [119] investigated the sensitive effect of top tension on the Vortex-Induced Vibration (VIV) of marine risers in deep waters using computational fluid dynamics (CFD). Other sensitivity investigations have been reported on fatigue life prediction of risers. These can be noticed in some sensitivity analyses on Steel Catenary Risers conducted on its Fatigue Behavior [120,121]. In the study by Yang & Li [121], the sensitivity analysis on the fatigue life of Steel Lazy Wave Catenary Risers (SLWR) conducted was motivated by the major consideration encountered while evaluating the practicality of using SLWR on large motion vessels like semi-submersibles and floating production storage and offloading (FPSOs) structures. There are other sensitivities reported in catenary sections and their impact along the touchdown zone [122,123]. Quéau et al. [123] presented some sensitivity investigations on fatigue damage of SCR dynamic loads in the touchdown zone by utilising a simple stress range evaluation framework. To improve the certainty on the design of SCR attached to deep-water FPSOs, a sensitivity analysis is also conducted by Yoo & Joo [124] under 1,400 m water depth for deep water environment in West Africa. Thus, the need for the investigation on the hydrodynamic characteristics, the wave-current interaction with the sensitivity studies of the attached hoses, and comparing the designs for Lazy-S and Chinese-lantern configurations, as performed in this present study.

The present paper presents the hydrodynamic characteristics with the sensitivity studies on CALM buoy with attached marine hoses. It was carried out using a developed numerical marine hose model under ocean environment with wave loads, as introduced in Section 1. Section 2 presents the materials and methods for the numerical model. The numerical model was developed using ANSYS AQWA R1 2021 [125-126] and Orcaflex 11.0f [127-130]. The modelled system included the submarine hoses attached to a floating CALM buoy structure, under waves and current. In this study, two representative configurations were considered, namely the Lazy-S and the Chinese Lantern configurations. A typical CALM buoy hose system is illustrated in Figures 2. Section 3 presents results and discussion, while further discussions on the studies were presented in Section 4. The concluding remarks are given in Section 5.

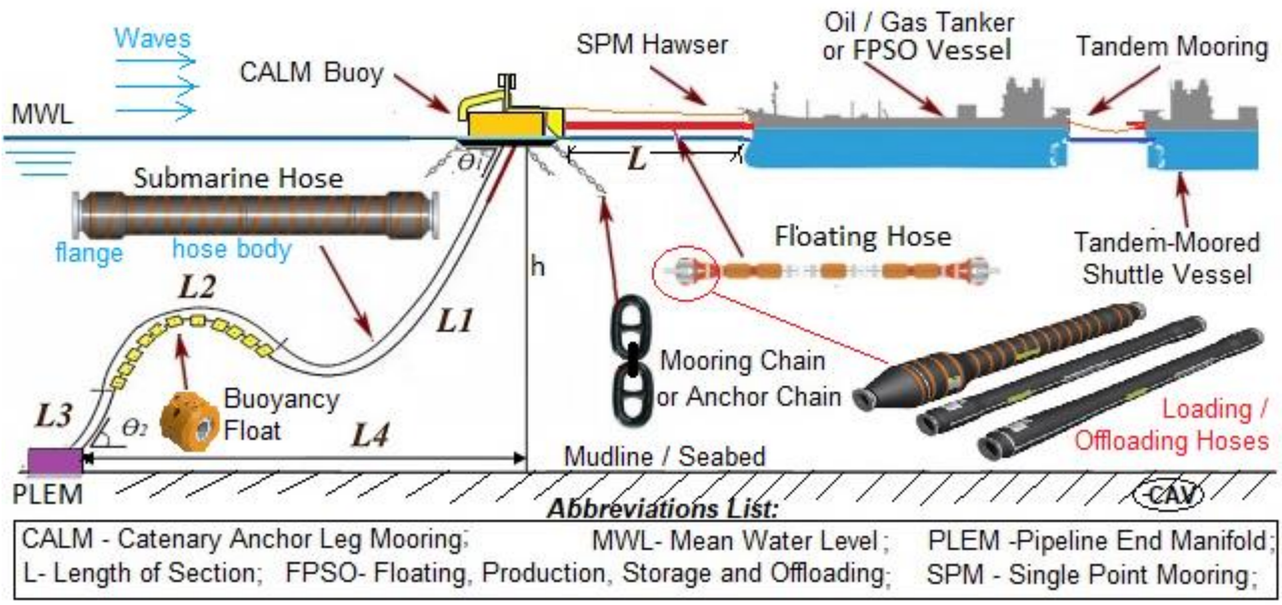


**Figure 2** Sketch showing the design parameters for a CALM buoy system with moorings, submarine hoses and floating hose. It shows loading and offloading operation on the CALM buoy in Lazy-S configuration, with wave forces and boundary conditions [Sketch design: by Author1- C.V.A].

## 2. Materials and Methods

The numerical modelling aspect has been presented in this section on the materials applied in this numerical model and the methodology. The materials include the buoy, submarine hoses, mooring lines and floats, as discussed in the subsequent sub-sections. The floating buoy considered in this study has six degrees of freedom (6DoFs), as depicted in Figure 3.

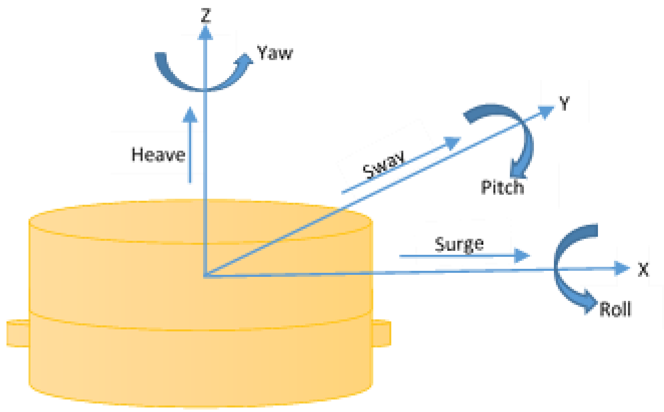


**Figure 3 The 6DoFs (six degrees of freedom) of a floating CALM buoy**

### *2.1. Buoy and Skirt Model*

The details for the buoy considered in this research are presented in Table 1. The hydrodynamics, hydrostatics and motion response of the CALM buoy was carried out for the cylindrical buoy (CB). The buoy's geometry was designed using Solidworks 2021. The description of the buoy geometry for the 1st concept of the CALM Buoy and skirt, showing (a) isometric view and (b) plan view is shown in Figure 4. This research also had a comparative study between different geometrical concepts and skirt concepts. Still, this paper is limited to one concept, as described herein, to present the advantage and justification. One vital use of this includes aiding designers in consideration of design parameters. The description for the buoy geometry shows the diameters, heights and locations of each part. It includes the CALM buoy body diameter $D_B$ and the CALM buoy skirt diameter $D_S$, the height of the buoy, $H_B$, the height of the skirt $H_S$, and the height from the keel to the underneath of the skirt, $H_K$. The model of the CALM buoy in Orcaflex is shown in Figure 5.

**Table 1 Parameters of the Buoy**

| Description | Value | Unit |
|---|---|---|
| Buoy Height | 4.50 | m |
| Draft | 2.40 | m |
| Water Depth | 100.00 | m |
| Buoy Mass | 198,834.00 | kg |
| Diameter of Buoy body | 10.00 | m |
| Diameter of Buoy Skirt | 13.90 | m |

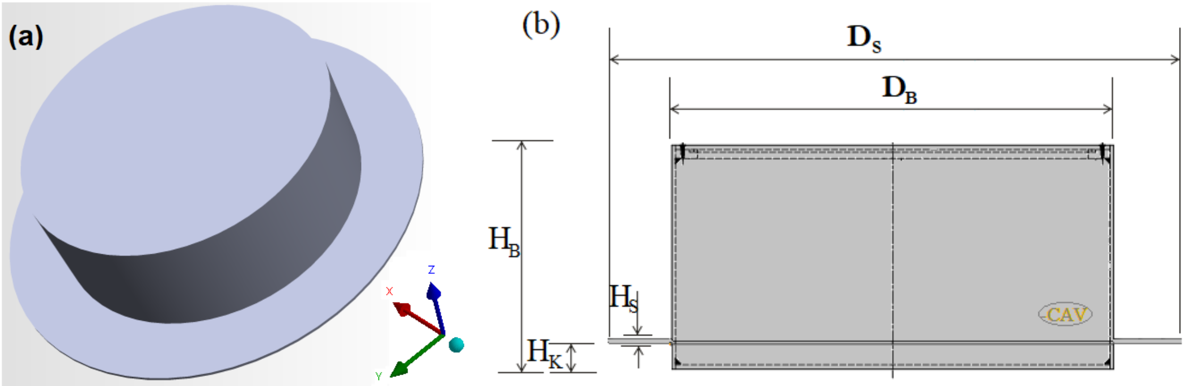


*Figure 4 Description of the geometry for the 1st concept of CALM Buoy and skirt, showing (a) isometric view and (b) plan view*

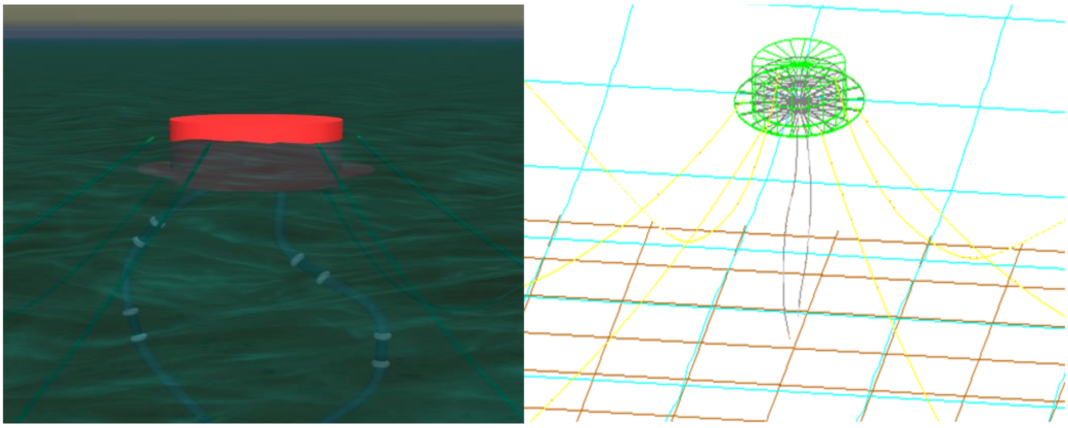

*Figure 5 Numerical model of the CALM Buoy showing (a)shaded and (b) wireframe views*

### 2.2. Submarine Hoses

The modelling consideration on the offshore submarine hose design were for an operation application with pressure rating of 19 bar (1,900KN/m$^2$). The offshore submarine hose was developed and modelled for two cases- Lazy-S and Chinese-lantern configuration, as illustrated in Figure 2(a-b). In each case, the two submarine hose strings are connected to the base of the buoy at the top and the Pipeline End Manifolds (PLEMs) at the bottom. The hoses are designed using existing current practices by hose manufacturers and industry end-users on oil fields [18,19,40-49]. For the Chinese-lantern configuration, the length of both submarine hose-strings were 25.90m per hose-string, as presented in Table 2. Whereas Lazy-S configuration, each submarine hoses were 162.065 m lengthwise, as presented in Table 3. The hose was assumed to be filled up and to contain completely-full fluid content. For the fluid content, it was tested with sea water of density 1,025kg/m$^3$ and with heavy oil of density 825 kg/m$^3$. Details of the parameters for the submarine hose considered are given in Table 2. The section profile for the submarine hose in Orcaflex 11.0f is depicted in Figure 6.

*Table 2 Parameters for the Submarine hose for Chinese-Lantern Configuration with section details arrangement*

| **Particulars** | **Description and Value** | | | **Unit** |
|---|---|---|---|---|
| Name | First-off Buoy hose | Mainline hose | First-off PLEM + floats | --- |
| Position of Part | 1st Section | 2nd Section | 3rd Section | --- |
| Hose Type Illustration | 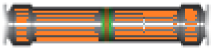 |  | 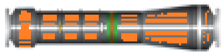 | --- |
| Hose Body Array | V1 (Hose Fitting) | V2 (Hose Fitting) | V3 (Hose Fitting) | --- |
| | V1 (Reinforced end) | V2 (Hose End) | V3 (Hose End) | --- |
| | V1 (Hose Body) | V2 (Hose Body) | V3 (Hose Body) | --- |
| | | V2 (Hose End) | V3 (Reinforced end) | --- |
| | V1 (Hose Fitting) | V2 (Hose Fitting) | V3 (Hose Fitting) | --- |
| Hose Section Mass | 239.00 | 495.00 | 239.00 | kg/m |
| Hose Outer Diameter, OD | 0.67 | 0.65 | 0.67 | m |
| Hose Inner Diameter, ID | 0.49 | 0.49 | 0.49 | m |
| Hose Length, L | 8.40 | 9.00 | 8.50 | m |

*Table 3 Parameters for the Submarine hose for Lazy-S Configuration with section details arrangement*

| **Section Number** | **Sub-Sections** | **Particulars** | **Inner Diameter (m)** | **Outer Diameter (m)** | **Section Length (m)** | **Segment Length (m)** | **Number of Segments** | **Unit Mass (kg/m)** | **Volume ($m^3$)** | **Segment Weight (N)** |
|---|---|---|---|---|---|---|---|---|---|---|
| Hose Group 1: Section 1 | 1 | Fitting | 0.489 | 0.650 | 1.0 | 0.800 | 1 | 495 | 0.330 | 492.5 |
| | 2 | Reinforced Hose End | 0.489 | 0.650 | 0.2 | 3.000 | 15 | 239 | 1.002 | 721.5 |
| | 3 | Hose Body | 0.489 | 0.650 | 0.5 | 3.236 | 6 | 180 | 1.074 | 582.5 |
| | 4 | Hose End | 0.489 | 0.675 | 0.5 | 0.895 | 2 | 200 | 0.320 | 179.0 |
| | 5 | Fitting | 0.489 | 0.650 | 1.0 | 0.800 | 1 | 495 | 0.330 | 492.5 |
| Hose Group 2: Section 2—Section 20 (same) | 6 | Fitting | 0.489 | 0.650 | 1.0 | 0.800 | 1 | 495 | 0.330 | 492.5 |
| | 7 | Hose End | 0.489 | 0.675 | 0.5 | 0.895 | 2 | 200 | 0.320 | 179.0 |
| | 8 | Hose Body | 0.489 | 0.650 | 0.2 | 3.840 | 19 | 180 | 1.274 | 691.2 |
| | 9 | Hose End | 0.489 | 0.675 | 0.5 | 0.895 | 2 | 200 | 0.320 | 179.0 |
| | 10 | Fitting | 0.489 | 0.650 | 1.0 | 0.800 | 1 | 495 | 0.330 | 492.5 |
| Hose Group 3: Section 21 | 11 | Fitting | 0.489 | 0.650 | 1.0 | 0.800 | 1 | 495 | 0.330 | 492.5 |
| | 12 | Hose End | 0.489 | 0.675 | 0.5 | 0.895 | 2 | 200 | 0.320 | 179.0 |
| | 13 | Hose Body | 0.489 | 0.650 | 0.5 | 3.236 | 6 | 180 | 1.074 | 582.5 |
| | 14 | Reinforced Hose End | 0.489 | 0.670 | 0.2 | 3.000 | 15 | 240 | 1.064 | 724.6 |
| | 15 | Fitting | 0.489 | 0.650 | 1.0 | 0.800 | 1 | 495 | 0.330 | 492.5 |

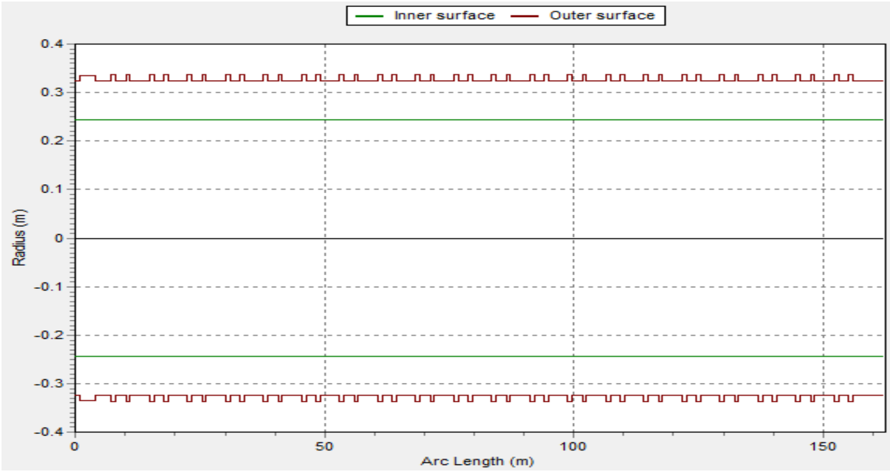


***Figure 6 Submarine Hose Profile showing the radii for inner and outer surfaces in Orcaflex***

### *2.3. Mooring Lines*

The mooring arrangement is 6 mooring lines positioned strategically at 60˚separation distance apart, to avoid line clashing. The schematic for the two configurations investigated are presented in Figures 2 and 7. Details of the mooring line parameters are detailed in Table 4. Each mooring line has the same stiffness. They are deployed as catenary mooring lines. For the arrangement, each mooring line is made up of two sections of steel chains. Two different materials were investigated on the mooring lines using steel chain and polyester mooring lines. Also, two different configurations for the section ratio were used: 150:195 and 50:175. The 2.5" mooring chain has a mass per unit length of 0.088 te/m (te: metric tonne). In Orcaflex ([127-130]), the bending stiffness is set to zero for both the studlink and the studless chains. In Table, $C_m$ denotes inertia coefficient, which is relates to $C_a$, the added mass coefficient, as expressed in Equation (1).

$$C_m = 1 - C_a \qquad (1)$$

**Table 4 Parameters for the Mooring Lines**

| **Description** | **Value** | **Unit** |
|---|---|---|
| Coefficient of Drag, $C_d$ | 1.00 | --- |
| Coefficient of Inertia, $C_m$ | 1.00 | --- |
| Section Lengths Ratio for 1st config. | 150:195 | --- |
| Section Lengths Ratio for 2nd config. | 50:175 | --- |
| Poisson Ratio | 0.50 | --- |
| Mass Per Unit Length | 0.088 | te/m |

| | | |
|---|---|---|
| Contact Diameter | 0.229 | m |
| Nominal Diameter | 0.120 | m |
| Bending Stiffness | 0.00 | N*m$^2$ |
| Axial Stiffness, EA | 407,257.00 | kN |
| Separation Distance between lines | 60 | ° |

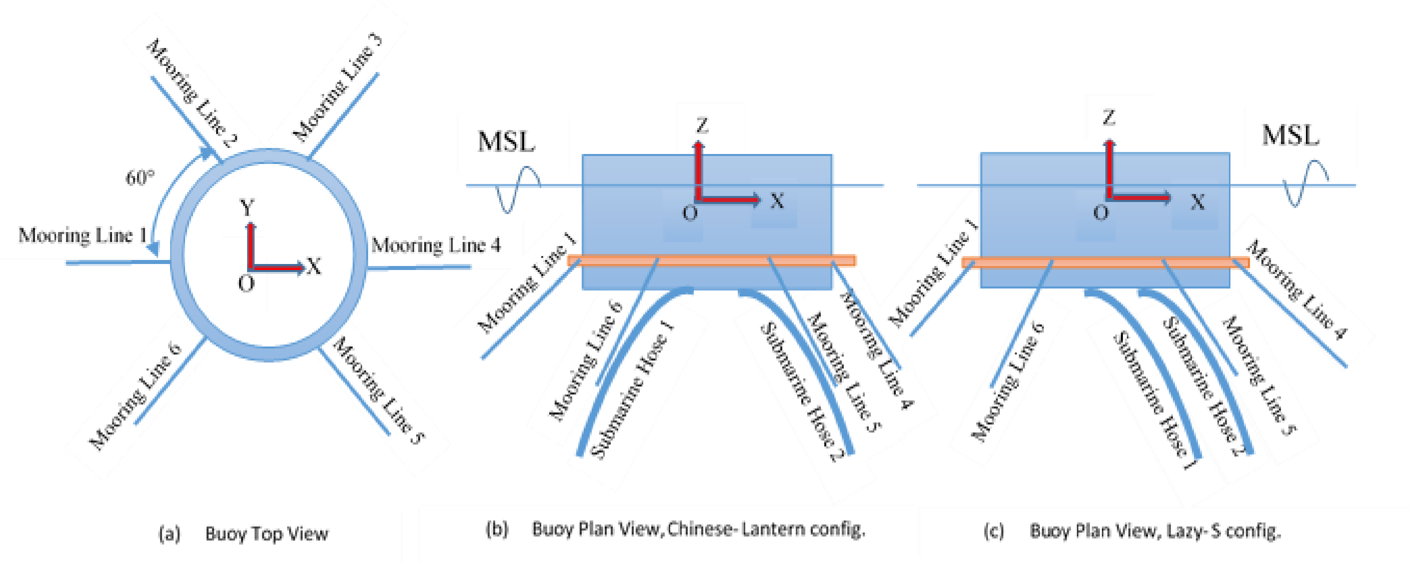


**Figure 7 Schematic for the mooring Lines on the buoy showing (a) Chinese-lantern, and (b) Lazy-S configurations**

*2.4. Buoyancy Float*

With a float incorporated as part of the hose line, the buoyancy connection on the hoses was designed. The design and construction of the float materials are per the OCIMF industry requirements [19,34-36]. The parameters for the buoyancy float are shown in Table 5. The buoyancy of the submarine hose line is obtained by designing a series of floats arranged together, as depicted in Figure 8.

In principle, submarine hoses are classified as slender bodies, and the floats are usually attached on them. The damping for the submarine hose can be evaluated by applying the modified Morison Equation [78], given in Equation (2), where D is the diameter of the body, $V$ is the volume of the body, $V_r$ is the relative velocity of fluid particles, $A$ is the area of the body, $C_a$ is the added mass coefficient, $C_d$ is the drag coefficient and $C_m$ is the inertial force coefficient.

$$F = \rho V \dot{u} + \rho C_a D A(V_r) + \frac{1}{2}\rho C_d A(V_r)|V_r| \quad (2)$$

However, for the floats, the principle of hydrodynamic equivalence is applied. With the application of equivalence principle of the hydrodynamic loads per unit length and buoyancy load for the buoyancy section as presented in [131], an expression for the equivalent float weight $w_e$, equivalent float outer diameter $D_e$, and equivalent hydrodynamic coefficients $C_{de}$ and $C_{\tau e}$ for the buoyancy section can be presented as Equations (3)-(6); where $w$ is the weight per unit length of riser, $l_f$ is the length of float, $v_f$ is the volume of float, $S_f$ is the float pitch, $\rho_f$ is the material density of buoyancy block, $m_f$ is the mass of float line considered, $F_{df}$ is the damping force of float, $m_{fh}$ is the mass of attached rigging hardware of buoyancy float block (like bolts, fixing clamps, etc.), $D_{ol}$ is the outer diameter of the derived hoseline and $C\tau n$ is the tangential drag coefficient acting on the cross section of buoyancy float block. The equivalent normal and tangential added mass coefficients for the buoyancy section can refer to the equivalent process of drag force coefficients [127-131]. The drag force per unit length of the derived hoseline, $F_{df}$ when flow is normal to the line's axis along the local x-direction is given by Equation (3);

$$F_{df} = \frac{1}{4}\left[\rho_f V_f^2 C_{df}\left(D_f^2 - D_o^2\right)\right] \quad (3)$$

$$D_e = \sqrt{\left({D_f}^2 - {D_o}^2\right).\left({}^{L_f}/_{S_f}\right) + {D_o}^2} \quad (4)$$

$$C_{de} = \frac{C_d}{D_e S_f}\left[D_f L_f + D_o\left(S_f - L_f\right)\right] \quad (5)$$

$$C_{\tau e} = \frac{1}{D_e S_f}\left[\frac{C_{\tau n}}{4}\left({D_f}^2 - {D_o}^2\right) + C_{dt} D_f L_f + C_{dt} D_o\left(S_f - L_f\right)\right] \quad (6)$$

The mass of each float, $m_f$ can be obtained by using the following expression in Equation (7), where ϱf denotes the density of the float:

$$m_f = v_f \rho_f + m_f \quad (7)$$

The numerical model considers the entire hose-string in deriving the mass per unit length, m for a line having floats by using the float distribution through the line and the corresponding value of the type of base line having mass, $m_l$, thus;

$$m = m_l + \frac{m_f}{S_f} \quad (8)$$

The volume of a single float, $v_f$ can be calculated using the following equation:

$$v_f = \frac{\pi}{4}\left({D_f}^2 - {D_o}^2\right).L_f \quad (9)$$

The volume per unit length of the hoseline with floats, $v_{lf}$ is obtained using:

$$v_{lf} = \frac{\pi}{4}{D_{ol}}^2 + \frac{v_f}{S_f} \quad (10)$$

**Table 5 Parameters for the Buoyancy Floats**

| Item | Value | | Item | Value |
|---|---|---|---|---|
| Classification of Float | Standard float | | Unit Mass, w (kg) | 102.00 |
| Float Type | Bolted type | | Net Buoyancy, $b_f$ (kg) | 280.00 |
| Filling Material | Polyurethane foam | | Outer Diameter, $D_o$ (m) | 1.23 |
| Metal Part Material | Stainless Steel | | Inner Diameter, $D_f$ (m) | 0.799 |
| Shell Material | Polyethylene | | Length of Float, $L_f$ (m) | 0.60 |
| Number of floats | Depends on config. | | Pitch of Floats, $S_f$ (m) | 2.00 |

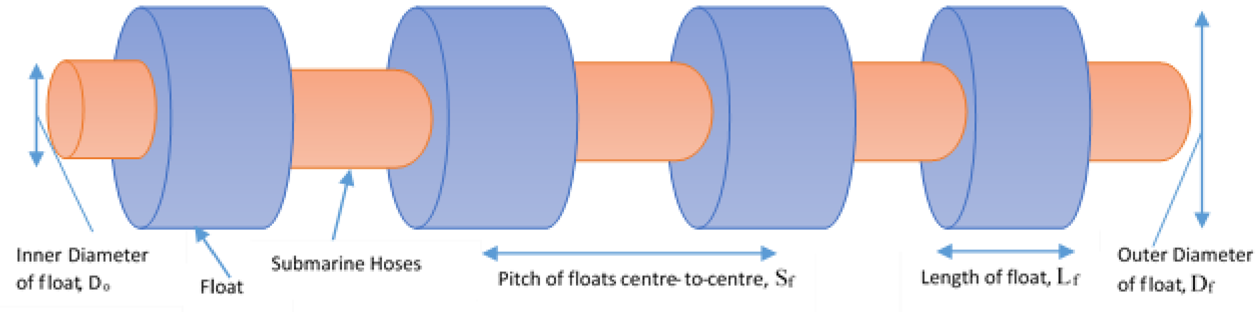


**Figure 8 Typical floats attached to offshore submarine hoses**

## *2.5. Analysis Method*

The methodology applied in this numerical modelling is based on commercial software tools for offshore ocean modelling, some semi-empirical calculations, and comparative sensitivity studies. The methodology for the analysis in this research is conducted in stages, as presented in Figure 9. The first set of studies were on the buoy analysis - mesh convergence, hydrostatics, and hydrodynamics. Next is the buoy motion study for the 6DoF. It was used to obtain the motion characteristics of the motion RAOs, added mass, radiation damping, first-order wave exciting forces, and second-order drift forces. It was then followed by the hose analysis for the sensitivity studies. After that, a comparative study on the coupled modelling of ANSYS AQWA and Orcina's Orcaflex 11.0f was conducted. The study's analysis method also involved both static and dynamic analysis. It was performed by carrying out the hydrodynamic analysis of the floating buoy using ANSYS AQWA R1 2021. The amplitude values for the motion called motion RAOs are then loaded into Orcaflex 11.0f. The results of the numerical investigation and the sensitivity analysis are presented in Section 3.

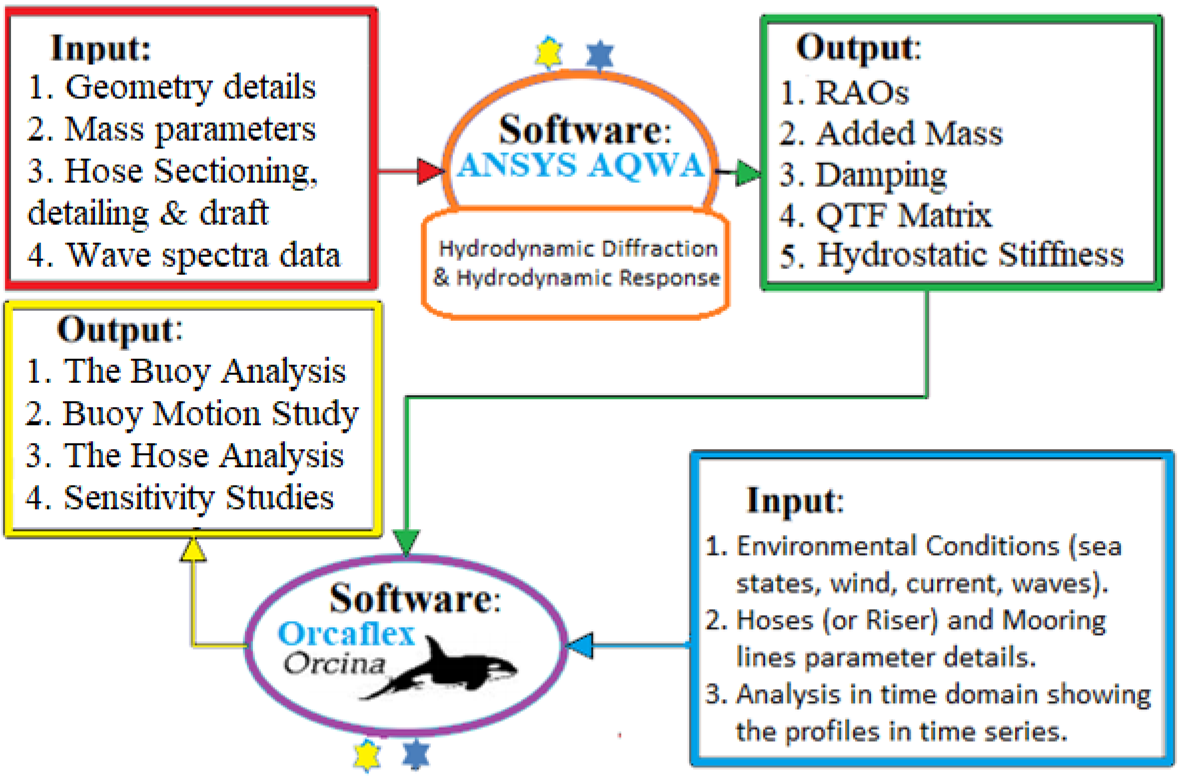


*Figure 9 The methodology for the sensitivity studies in the numerical modelling*

## *2.6. Hose Load Cases*

For the investigation, the full time for a fully developed sea (fds) of 10,800s (3 hours) in real-time was used for each simulation run in the Orcaflex analysis with early hose disconnect also considered, as seen in the higher curvature results for extreme cases. For the hose analysis, the numerical investigation is conducted using the mooring load cases in Table 6. Based on global loadings, operational conditions were first considered. In this purview, operation conditions means when the submarine hoses are connected to the CALM buoy, and the six mooring lines are utilised to moor the CALM buoy to the seafloor, as shown in Figure 5. The research aim is on two conditions -operating and survival.

The complete operation -loading and offloading, are not included in this study. Figure 10 is an illustrative description for the mooring conditions with the load cases applied in the hose analysis, showing (a) damaged mooring line 01 (ML01), (b) damaged mooring line 06 (ML06), and (c) intact mooring lines. The operation case considered is the third case whereby the moorings are intact and in healthy condition. This study does not consider the whole operation, including the connection of the oil tanker to the CALM buoy and the hawser lines, as the study is limited to buoy motion and submarine hoses. The worst-case scenario for harsh conditions is calculated using the buoy offsets, mooring configuration, and key environmental heading. For both wind and current, the 100-year extreme wind condition is taken into account. The combination of the wind, current, and waves are shown in Figure 10.

**Table 6 Load Case for Hose Analysis**

| Condition | Mooring | Tanker | Heading | Configuration |
|---|---|---|---|---|
| Operation | Damage | Yes | In-line | Lazy-S |
| | | Yes | In-between or Cross | Chinese-lantern |
| | Intact | Yes | In-line | |
| | | Yes | In-between or Cross | |
| Survival | Damage | Yes | In-line | Lazy-S |
| | | Yes | In-between or Cross | Chinese-lantern |
| | Intact | Yes | In-line | |
| | | Yes | In-between or Cross | |
| Extreme | Damage | No | In-line | Lazy-S |
| | | No | In-between or Cross | Chinese-lantern |
| | Intact | No | In-line | |
| | | No | In-between or Cross | |

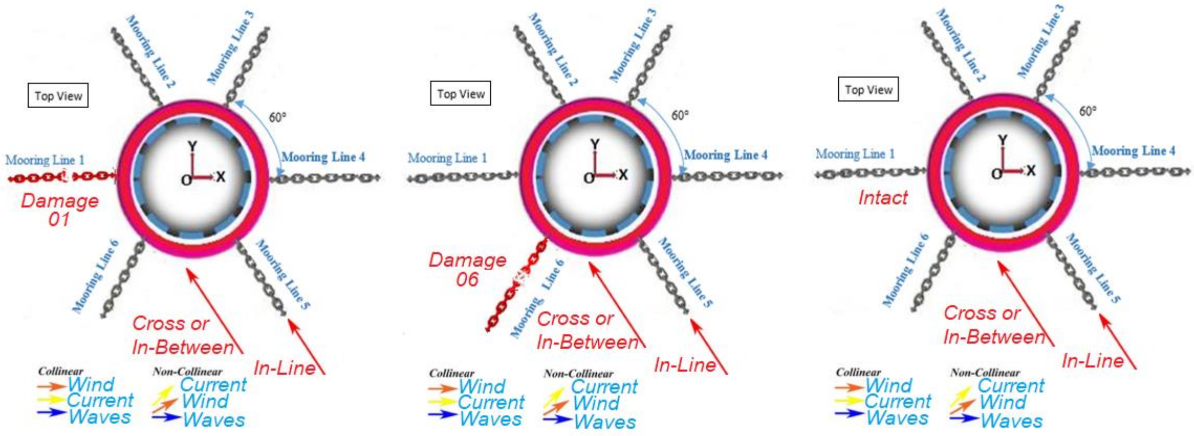


*Figure 10 The description of the mooring conditions for the load cases applied in the hose analysis, showing (a) damaged mooring in ML01, (b) damaged mooring in ML06, and (c) intact mooring*

### 2.7. FEM modelling

The Finite Element Model (FEM) for the CALM buoy hose system was designed in an ocean environment. Irregular waves under fully-developed sea were utilised. The design of the hoses is based on simple beam theory, and later using Orcaflex line theory in Orcaflex version 11.0f [127-130]. Orcaflex applies line theory considers line elements and lumped mass at each section nodes, as shown in Figure 11(a-c). For submarine hoses, the element type that it also applies is lines. Basically, this type of element is flexible with permissions for force displacements in bending, torsion and tension. Details on the principle of line theory used in the FEM of the submarine hose lines and the mooring lines are presented in [127-130]. The validity of this FE model in this research is also conducted by comparing results of finite element analysis and analytical analysis, as conducted in Section 2.11. Table 7 presents the details for the ocean. The system was tensioned using a mooring configuration consisting of six moorings. It was then affixed to the anchor and attached to the body of the buoy skirt. Catenary equations were used to compute the statics of the mooring lines and the submarine hoses (see Section 2.11). The finite element model for the CALM buoy model as depicted in Figures 12(a-b), in Orcaflex shows different components.

*Table 7 Parameters for the Ocean and Seabed*

| Item | Value | Unit |
|---|---|---|
| Ocean Temperature | 10 | °C |
| Ocean Kinematic Viscosity of Ocean | $1.35 \times 10^{-6}$ | $m^2s^{-1}$ |
| Density of Water | 1,025 | $kgm^{-3}$ |
| Wave Amplitude | 0.145 | m |
| Seabed Stiffness | 7.5 | $kNm^{-1}m^2$ |
| Seabed Shape Direction | 0 | ° |
| Water Depth | 26.0m (Chinese-lantern) and 100.0m (Lazy-S) | m |
| Seabed Friction Coefficient | 0.5 | --- |
| Seabed Model Type | Elastic Linear & Rigid Nonlinear Soil Models | --- |

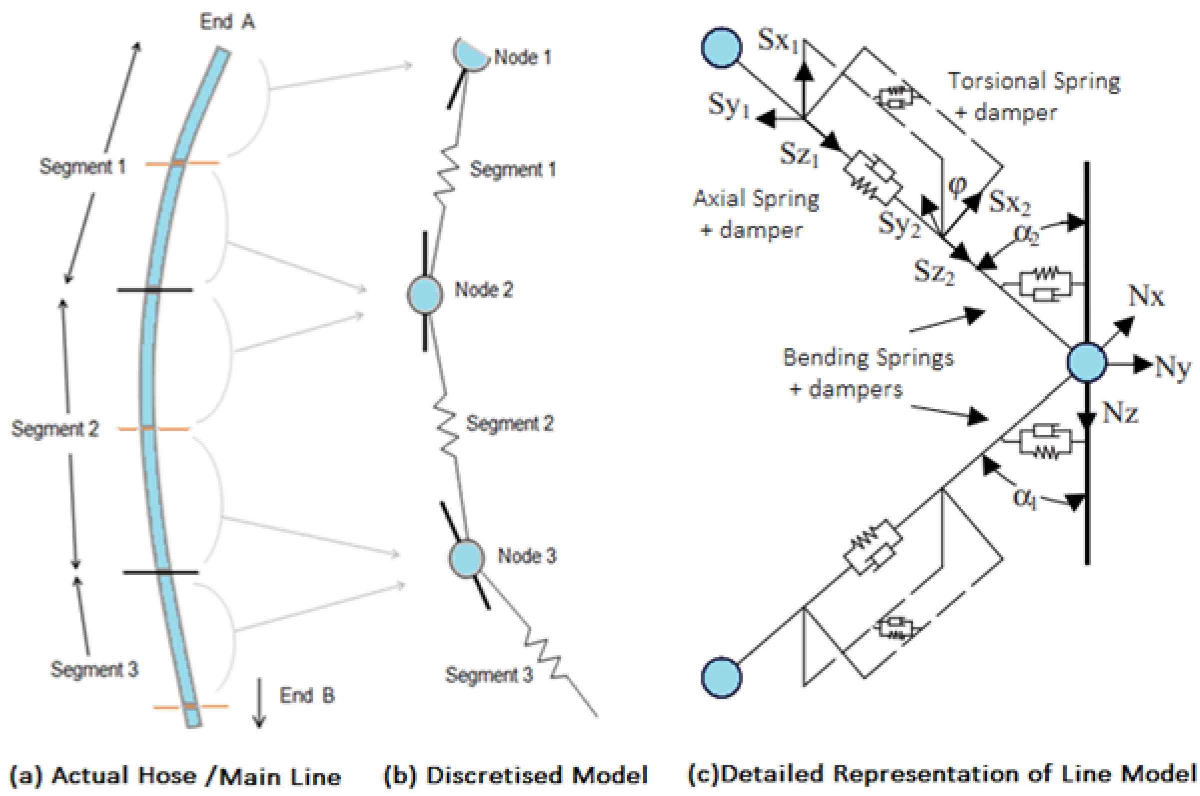


*Figure 11 The Orcaflex Line Theory depicting (a) actual main hose line, (b) discretized model and (c) detail representation of the Line Model (Adapted, courtesy of Orcina, 2014; 2020; 2021)*

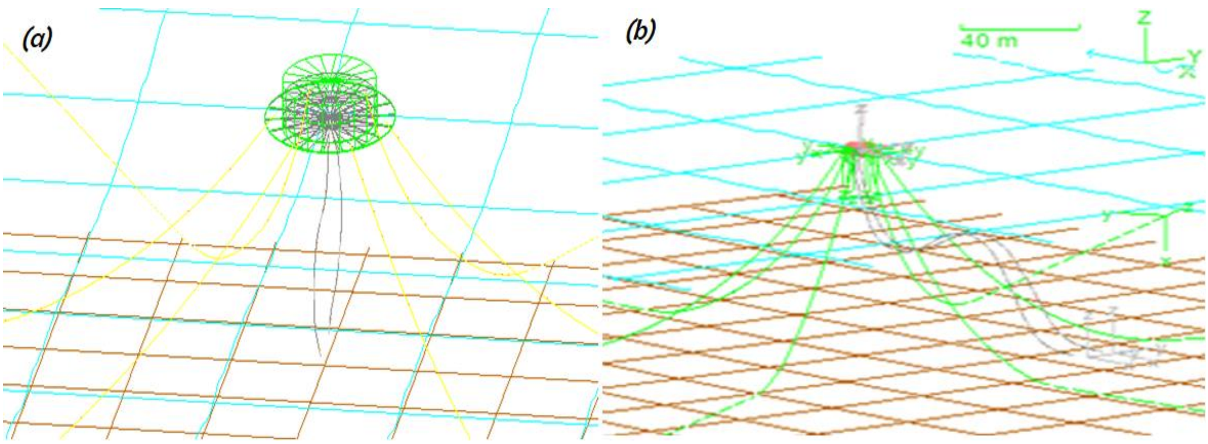


***Figure 12 CALM buoy finite element model of (a) Chinese-lantern and (b) Lazy-S configurations***

### *2.8. Environmental Conditions*

The modelling for the floating buoy is for operation in an ocean environment. The buoy is acted upon by some loadings, including waves, currents, and other hydrodynamic forces. It was modelled according to recommendations of industry standards [132-135]. The environmental conditions for the three sea states considered for the global loading and this analysis are presented in Table 8. Figure 13 shows the JONSWAP wave spectrum for the (a) 1st Sea state and (b) 3rd Sea States considered in this investigation. It shows that the input wave conditions with different wave periods have different peak frequencies. The wave heading with a description of the wave angles is presented in Figure 14. A uniform current profile was considered for the load estimation, and wind loads were added to the CALM buoy model. The current speed employed was 0.5 m/s while the wind speed was 22 m/s, respectively. The current profile for the surface current and seabed current in the X-Y axes is detailed in Table 9. The wave spectra adopted for the investigation is the JONSWAP (Joint North Sea Wave Project) Spectrum. This spectrum accounts for any imbalance in the energy flow within the wave system. Equation (11) is the JONSWAP spectrum [136-140], where $\omega$ is the angular frequency, $\omega_p$ denotes the peak angular frequency, g denotes gravitational constant for gravity, η denotes the incident wave amplitude, γ denotes the peak enhancement factor, while the other parameters σ, $\sigma_1$, $\sigma_2$ are spectral width parameters. These are also dependent on the significant wave height, $H_s$, and the zero-crossing period, $T_z$. According to findings in literature, ([127-129,140]) using Equations (11)-(15), the following are constants for sigma; $\sigma_1 = 0.07$, and $\sigma_2 = 0.09$.

$$S_\eta(\omega) = \frac{\alpha g^2}{\omega^5} exp\left[-\frac{5}{4}\left(\frac{\omega_p^4}{\omega^4}\right)\right]\gamma^a \quad (11)$$

$$S_\eta(\omega) = \frac{\alpha g^2 \gamma^a}{\omega^5} exp\left[\left(-\frac{5}{4}\frac{\omega_p^4}{\omega^4}\right)\right] \quad (12)$$

$$a = exp\left[-\frac{1}{2\sigma^2}\left(\frac{\omega_p}{\omega} - 1\right)^2\right] \quad (13)$$

$$\sigma = \sigma 1 \text{ for } \omega_p \le \omega \quad (14)$$

$$\sigma = \sigma 2 \text{ for } \omega_p > \omega \quad (15)$$

These are also dependent on the zero-crossing period, $T_z$ and the significant wave height, $H_s$. The JONSWAP Spectrum is a modified from Pierson-Moskowitz spectrum [141], to take care of regions that have geographical boundaries so as to limit the fetch as regards the wave generation. With modifications made to the JONSWAP equation, better capturing was made in regions with geographical boundaries that had limit on the fetch during the generation of waves.

*Table 8 Wave Parameters for the 3 load Cases*

| Case No. | $H_S$ (m) | $T_Z$ (s) | $T_P$ (s) | Conditions | Wave Angles (°) | Hydrodynamic Loads (HL) |
|---|---|---|---|---|---|---|
| 01 | 1.87 | 4.40 | 5.50 | Operation | 0,30,60,90,120 | Coupled (has HL), Uncoupled (no HL) |
| 02 | 2.40 | 6.10 | 7.85 | Extreme | 0,30,60,90,120 | Coupled (has HL), Uncoupled (no HL) |
| 03 | 4.10 | 5.50 | 9.65 | Survival | 0,30,60,90,120 | Coupled (has HL), Uncoupled (no HL) |

*Table 9 Wind and Current Parameters*

| Item | Value | Unit |
|---|---|---|
| Current Direction | 180.00 | ° |
| Surface Current | 0.50 | $ms^{-1}$ |
| Seabed Current | 0.45 | $ms^{-1}$ |
| Wind Speed | 22.00 | $ms^{-1}$ |
| Wind Type | Constant | --- |
| Density of Air | 1.225 | $kgm^{-3}$ |
| Kinematic Viscosity of Air | 0.000015 | $m^2s^{-1}$ |

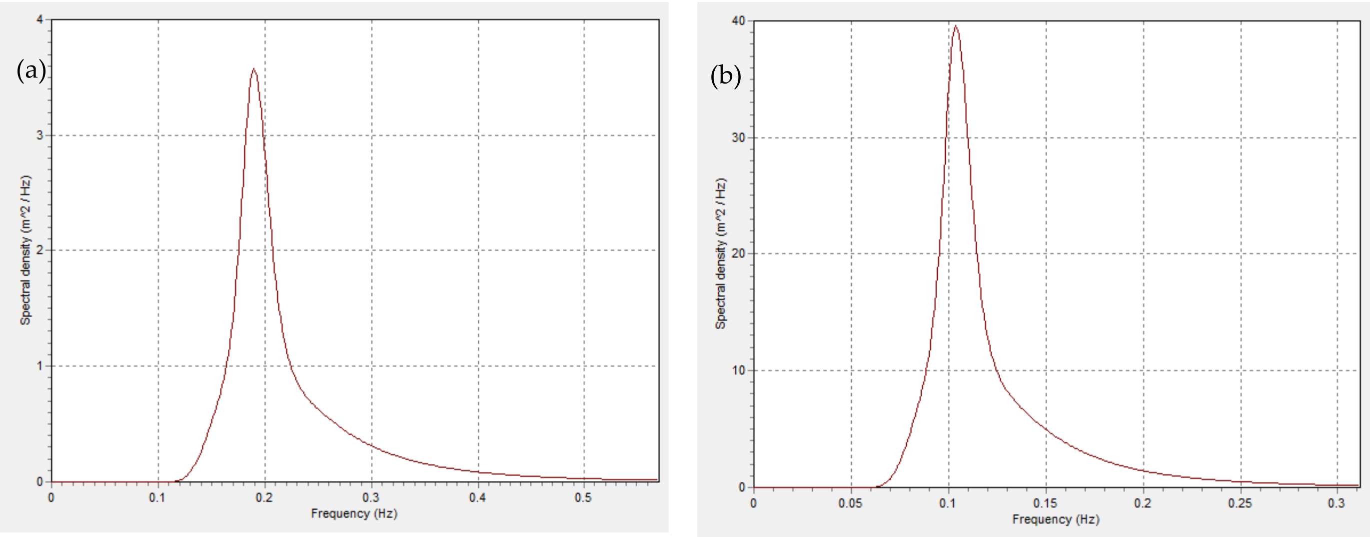


**Figure 13 The JONSWAP wave spectrum for the (a) 1st Sea state and (b) 3rd Sea States**

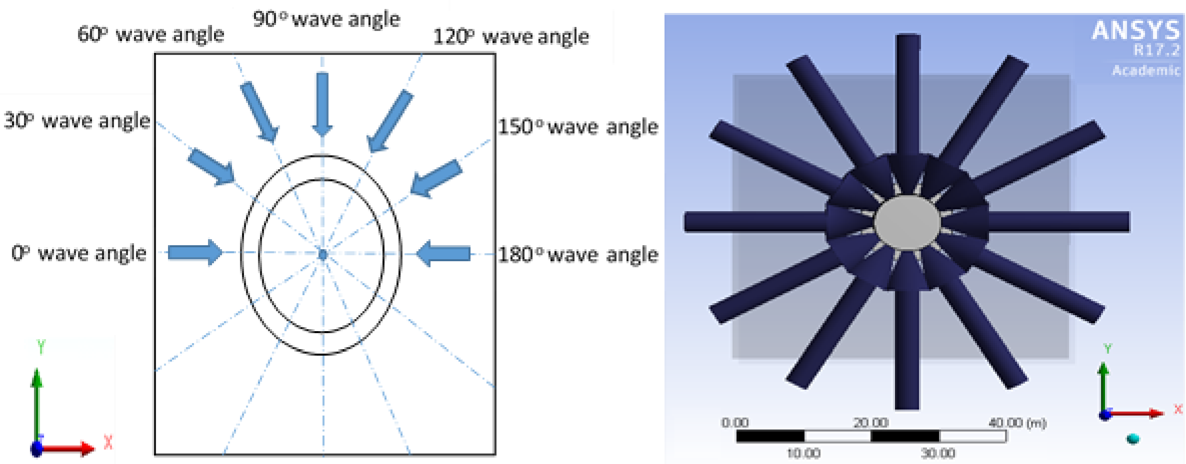


**Figure 14 Definition of Wave Angles on the buoy at 30° interval showing wave heading**

## *2.9. Buoy Hydrostatics*

The details for the buoy hydrostatics are given in Table 10. The local cartesian coordinate system was considered in the numerical model. Since the RAOs represent the floater behaviour with buoy hydrostatics, the motion characteristics from the RAOs generated were loaded into the Orcaflex model. The hydrostatic aspect of the numerical model was applied in the buoy for the coupled dynamic analysis using Orcaflex 11.0f. The buoy's AQWA hydrodynamics/panel model was free, without any mooring line and hoses attached to it, as similarly applied in other offshore structures. Details of the stiffness matrix for the buoy are presented in the literature [1]. In obtaining the RAOs, the mooring lines and hoses were not included in the ANSYS AQWA model. The models are validated in Section 2.11. Then, it was used in conducting sensitivity studies with the validated numerical model of the CALM buoy hose system. Figure 15 depicts the model ocean view of the CALM buoy in free-floating mode for hydrodynamic and hydrostatic analysis. The dimension for the model box is 150m × 150m, and the box illustrates the X and Y directions of the sea conducted under fully developed sea conditions.

**Table 10 Parameters for the Buoy Hydrostatics**

| Item | Value | Unit |
|---|---|---|
| Buoy Area | 438.49 | $m^2$ |
| Buoy Volume | 344.98 | $m^3$ |
| $I_{xx}$ (Moment of Inertia) | 4,331,379.37 | $Kg.m^2$ |
| $I_{yy}$ (Moment of Inertia) | 4,486,674.11 | $Kg.m^2$ |
| $I_{zz}$ (Moment of Inertia) | 4,331,379.37 | $Kg.m^2$ |
| CoG (Centre of Gravity) | -2.20 | m |
| $B_f$ (Buoyancy Force) | 1,967,500.00 | N |

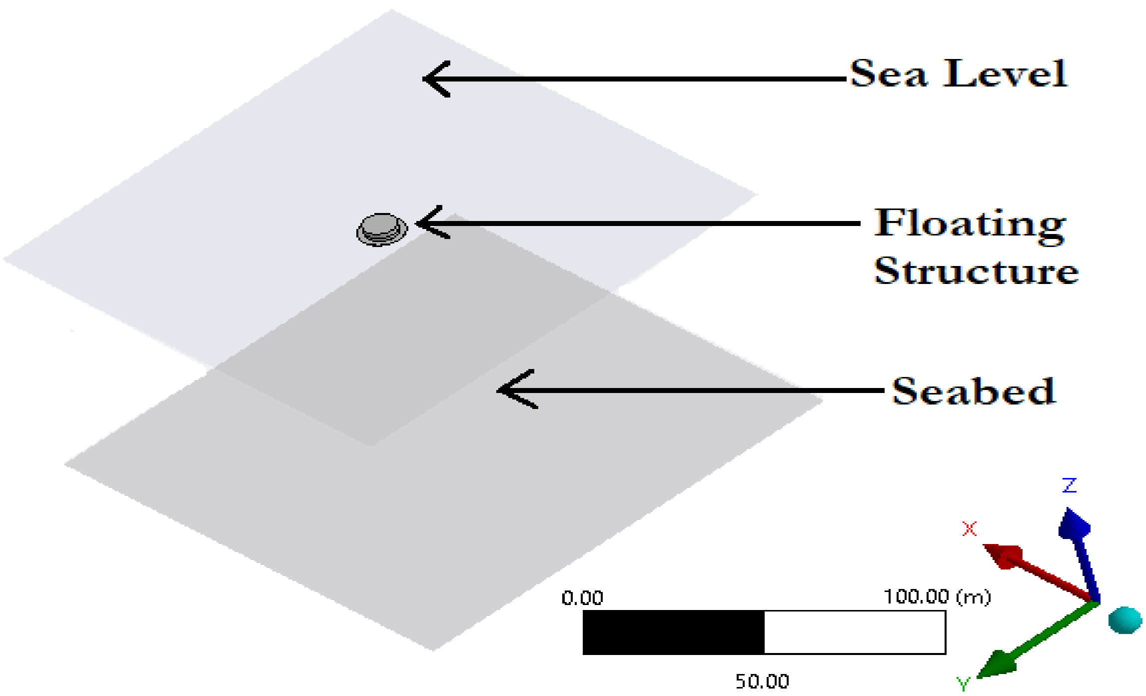


*Figure 15 Model Ocean View of the free-floating CALM Buoy in ANSYS AQWA R1 2021*

## *2.10. Mesh Convergence*

An extensive mesh convergence analysis in the diffraction study in ANSYS AQWA R1 2021 was conducted to validate the numerical model. A value of tolerance considered is 0.01m and the highest element size considered was 1.25m. In order to confirm that the study was conducted using the best effective element size in meshing, the range of the elements selected were from 1.25m to 0.225m. The mesh study was investigated by utilising the panel model. This was conducted on the CALM buoy under the ocean environment to study the tension, surge displacement, and bending in the surge motion. The RAO values were obtained from the hydrostatic parameters such as potential damping and added mass. For the convergence study in Figure 16, a single wave angle $0^0$ was considered. Table 11 is the results obtained from the effect of the maximum surge RAO that acts along the $0^0$ incidences. From the statistical analysis, the maximum RAO variance and maximum RAO deviation were taken from 0.225m mesh size. The study showed very small deviations in the RAOs obtained from the maximum at 0.25m element size. Surge RAO is dimensionless, with unit as m/m, as seen in the convergence plot. Precisely, it is quite minimal and very much less than 3%, as observed in Table 11, which implies that the tolerated deviation considered in this analysis will save computational resources and be sufficient, acceptable, and validates this study.

**Table 11 Convergence Study using Surge RAO**

| **Mesh Size** | **Nodes** | **Elements** | **Surge RAO (m/m)** | **Max. RAO Variance from 0.225m** | **Max. RAO Deviation from 0.225m** |
|---|---|---|---|---|---|
| 0.225 | 38572 | 38570 | 0.90610 | 0.000000 | 0.00000% |
| 0.25 | 31554 | 31552 | 0.90605 | **0.000000** | 0.00004% |
| 0.35 | 16464 | 16462 | 0.90427 | **0.000016** | 0.00126% |
| 0.75 | 4070 | 4068 | 0.89206 | **0.000075** | 0.00863% |
| 1.25 | 1628 | 1626 | 0.87012 | **0.000241** | 0.01551% |

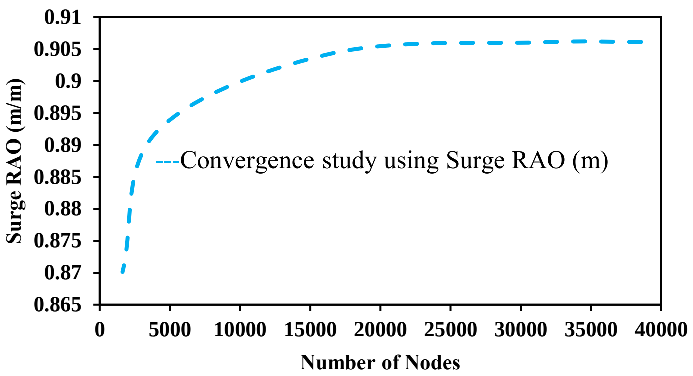


*Figure 16 Convergence Study on buoy using Surge RAO (m)*

### *2.11. Model Validation*

The validation considerations conducted on this study are presented in this section.

#### 2.11.1. **Numerical Model Validation**

The validity of this model was carried out by a comparison of theoretical and numerical computations on the marine hose models. The catenary method was utilised in the statics calculation for computing the submarine hose and that of the mooring lines. An illustration of the catenary line with the global coordinate system in X-Z plane is given in Figure 17. Using the notations on the sketch in Figure 17, the catenary equation is considered as expressed in Equation (16), where *H* is the horizontal tension component of the system, *w* is the weight per unit length, *z* is the catenary line parameter for the distance from the seabed to the top of the line, and *x* is the section length.

$$z = \frac{T_H}{w_s}\left[\cosh\left(\frac{x w_s}{T_H}\right) - 1\right] \qquad (16)$$

To obtain the curvature at sagbend, the tension components are required. The shape of the catenary can be obtained by calculation [60], using the expression in Equation (16). However, to compute the maximum curvature of the hoseline or mooring line at touch down point (TDP), Equation (17) can be applied:

$$\frac{1}{R} = \frac{w_s}{T_H} \qquad (17)$$

Where $w_s$ is the submerged weight per unit length of hose-string or mooring line, x is the section length from TDP, $T_h$ is the horizontal force acting at the seabed, and z is the height above seabed. Note that h and z can be used to depict vertical heights for top section and TDP, respectively. In this case, z is considered for uniformity.

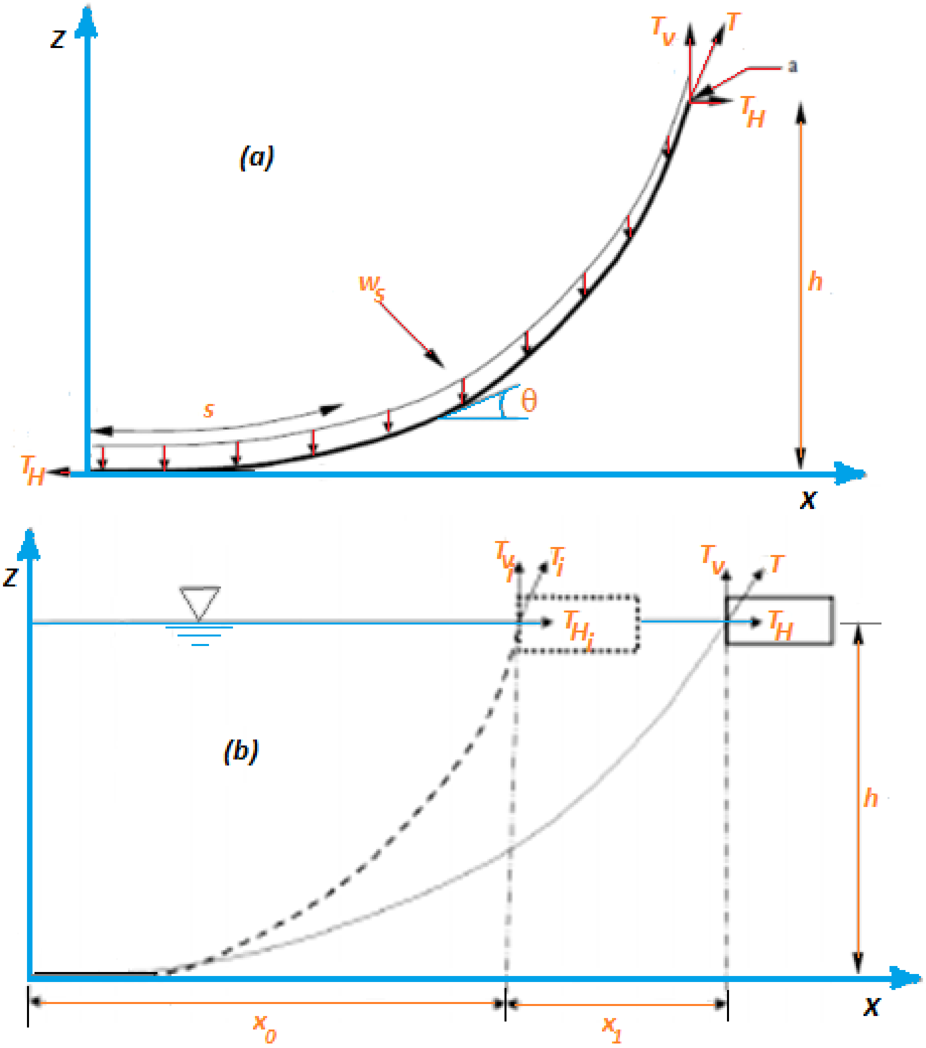


**Figure 17 Forces on the Catenary design of a mooring line, showing (a) static line and (d) line with offset**

The first validation approach considered comparisons between analytical and numerical results, which are acceptable by considering more perspectives. To obtain the vertical force, $T_v$ and the horizontal force, $T_H$ acting at the topmost hose-end, the expressions given in Equations (80) and (81) are the relationships for $T_H$ and $T_v$ obtained theoretically as the centenary equations [60,142-145], where *s* denotes the hose arc-length, $\theta$ denotes angle along the horizontal plane, $w_s$ denotes the submerged weight, and *z* denotes the height above seabed, thus:

$$T_H = \frac{z \cdot w_s}{(tan\,\theta)^2} \cdot (1 + \sqrt{[1 + (tan\,\theta)^2]}) \qquad (18)$$

$$T_v = s \cdot w_s \qquad (19)$$

The arclength for the hose top tension, $s_{top}$ and the arclength at the hose TDP (touch down point) tension, $s_{TDP}$ which relate to the arclengths in the horizontal and vertical components, can be obtained using Equations (20) and (21) respectively. Thus,

$$s_{top} = \mathrm{h} \cdot \sqrt{(1 + 2 \cdot \frac{T_H}{h \cdot w_s})} \qquad (20)$$

$$s_{TDP} = \mathrm{z} \cdot \sqrt{(1 + 2 \cdot \frac{T_H}{h \cdot w_s})} \qquad (21)$$

The angle between the hoseline or mooring line and the x-y plane is given by:

$$\tan\theta = \frac{\mathrm{T_H}}{\mathrm{T_v}} \qquad (22)$$

Based on this approach, validations of marine hoses were conducted using method in earlier study [146], considering the maximum tensions in horizontal and vertical components. It should be noted that components like bending moments and stress deformations generally reflect structural stiffness sometimes. For instance, pipeline deformation along the arc length during S-laying; although forces can be directly correlated to the deformations. Some analytical computations were conducted by hand-calculations to check the model. Table 12 presents the typical calculation conducted on the catenary mooring system.

*Table 12 Typical Calculation for Mooring line tension*

| **Calculation:** |
| --- |
| **Known：**<br><br>The equivalent density ($w_s$) of hose per unit length in air = 4789kg/m,<br>The submerged weight per unit, ($w_s$) is 5315kg/m.<br>Depart angle $\theta$ at the top = 30 degrees,<br>Depart angle $\theta$ at the TDP = 45 degrees,<br>Height above seabed, *h* of the hose = 1.495m |
| **Calculations at Top：**<br>Where $w_s$=5315kg/m; θ=30°; z=1.495m<br>Horizontal force $T_H = \frac{z \cdot w_s}{(\tan\theta)^2} \cdot (1 + \sqrt{(1 + (\tan\theta)^2)}) = 51363.267\mathrm{kg}$<br>Arclength $\mathrm{s} = \mathrm{h} \cdot \sqrt{(1 + 2 \cdot \frac{T_H}{h \cdot w_s})} = 5.579\mathrm{m}$<br>Vertical force $\mathrm{T_v} = \mathrm{w_s} \cdot \mathrm{s} = 29652.385\mathrm{kg}$ |
| **Touch down point(TDP):**<br>Where $w_s$=5315kg/m; θ=45°; z=0m<br>Horizontal force $T_H = \frac{z \cdot w_s}{(\tan\theta)^2} \cdot (1 + \sqrt{(1 + (\tan\theta)^2)}) = 0\mathrm{kg}$<br>Arclength $\mathrm{s} = \mathrm{z} \cdot \sqrt{(1 + 2 \cdot \frac{T_H}{h \cdot w_s})} = 0\mathrm{m}$<br>Vertical force $\mathrm{T_v} = \mathrm{w_s} \cdot \mathrm{s} = 0\mathrm{kg}$<br>If the acceleration of gravity, g=10N/kg,<br>**Top：** $T_H = 513.63267\mathrm{KN}; \mathrm{T_v} = 296.52385\mathrm{KN}$<br>**TDP：** $T_H = 0\mathrm{KN}; \mathrm{T_v} = 0\mathrm{KN}$ |

Table 13 shows the outcome from computations involving the numerical solutions using FEA and the analytical solutions using two hose parameters -horizontal tension and vertical tension. Based on the horizontal tensions have higher profiles for the analytical and finite element results, respective approximates as 109.30 kN and 115.40 kN. On the other hand, the vertical tension components, the analytical and finite element respective approximates are 81.60 kN and 78.50 kN. Table 13 shows good agreement betwixt the two approaches, with the deviation along the vertical tension path as 3.9% while the deviation along the horizontal tension path is 5.3%.

**Table 13 Validation by comparing the hose values for maximum tension components**

| **Model Description** | $T_v$,**Vertical Tension (KN)** | $T_h$, **Horizontal Tension (KN)** |
|---|---|---|
| Analytical Model (AM) | 81.60 | 109.30 |
| Finite Element Model (FEM) | 78.50 | 115.40 |
| Average Result = AM/FEM | 1.039 | 0.947 |

### 2.11.2. **Experimental Model Validation**

The second validation conducted was by considering the motion behaviour of the CALM buoy hose system with component design using an experimental model in Lancaster University wave tank facility, as shown in Figure 18. On the experimental model, four (4) sensors points were made and wave gauages attached. The buoy was restrained with four (4) mooring chains and two (2) model hoses were attached to the buoy.

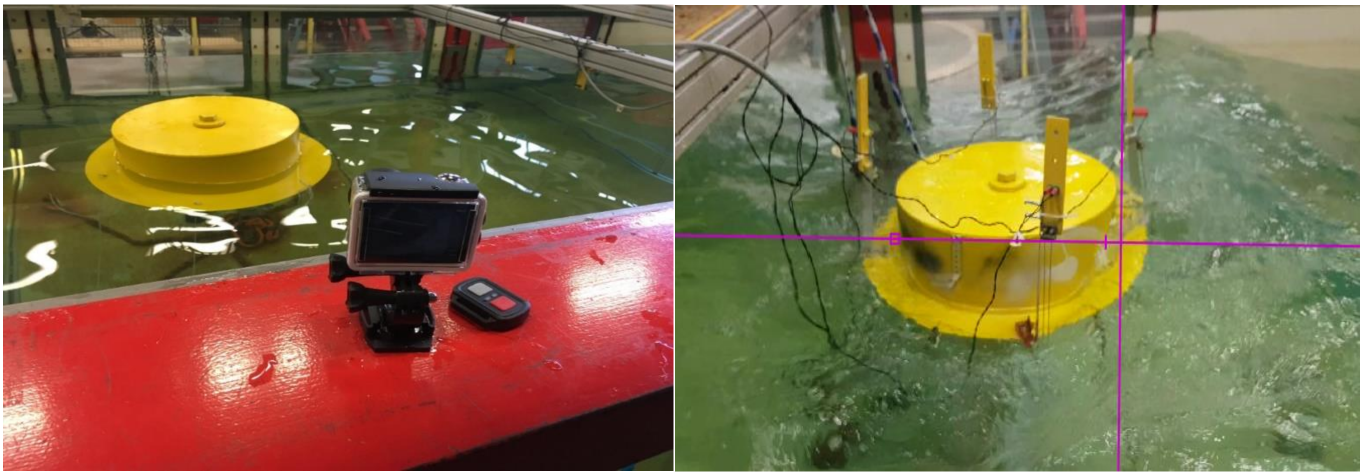

*Figure 18 CALM buoy model used in experiment in Lancaster University Wave Tank, showing (a) model setup with the underwater camera and (b) the model under wave run as postprocessed using Tracker software*

The experiment was carried out on Lancaster University Wave Tank using CALM buoy model as shown in Figure 19. The wave tank is 12.5 metres long, 2.5 metres wide, and 1.7 metres deep, as indicated in Figure 20. The waves are created with the help of seven flappy-type paddles made by Edinburgh Designs, U.K. Each paddle can generate sinusoidal waves with frequencies ranging from 0.5 to 1.5 Hz and amplitudes of up to 100 mm. Depending on the input setup, they can generate both regular and irregular waves from data files. As shown in Figure 21, the model test was built with two undersea hoses attached beneath the buoy. The CALM buoy test model was first evaluated for buoyancy and leakage before being ballasted properly. It was then placed on the wave tank's middle line, 5.5 metres from the wave maker. An Akaso EK7000 waterproof-underwater camera with Ultra High Definition (HD) 4K image quality and a 170° wide vision was used to record video for each run. For various frequencies, it recorded the behaviour of the submarine hoses and the CALM buoy. For the first round of the experiment, multiple frequencies were tested on a flat seafloor. The readings are obtained using a set-up with LabView NXG 5.1 and wave gauges. The LabView was connected to a National Instruments DSUB Model NI 9205 NI-DAQmx Device. Both ends of the two undersea hoses attached to the buoy model were fitted with end-fittings. The mooring lines were composed of steel chains with a diameter of 20mm, with one end secured to the floor and the other to the skirt of the CALM buoy model. Each of the 4 Wave Gauges attached to the buoy had a maximum signal input of 5 volts (WG1- WG10).


**Figure 19 Lancaster University wave tank showing the test basin with location of buoy and wave gauges**

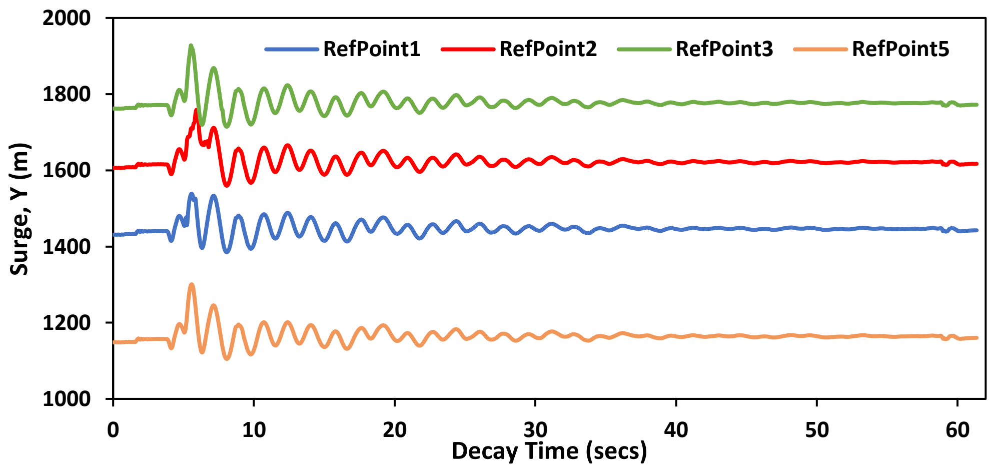


*Figure 20 Surge motion for Decay Test of the CALM Buoy using the DIC with Imetrum System at 62secs run*

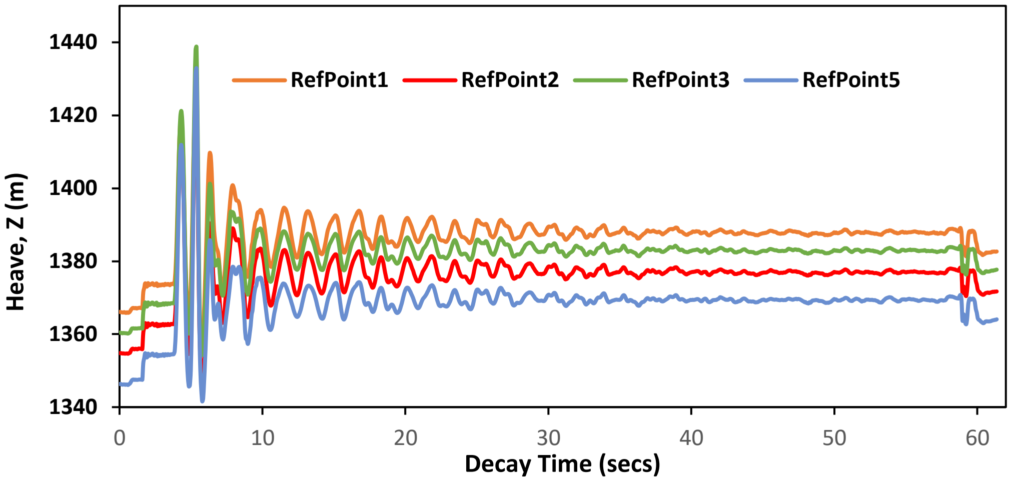


*Figure 21 Heave motion for Decay Test of the CALM Buoy using the DIC with Imetrum System at 62secs run*

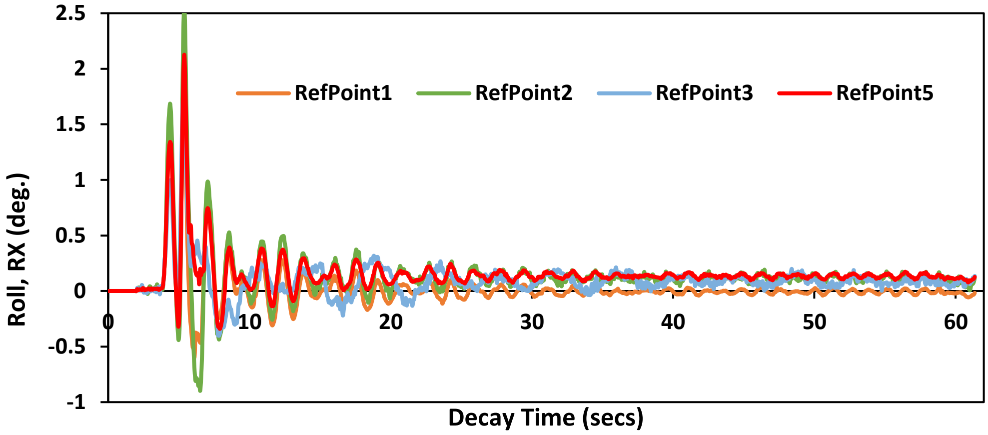


*Figure 22 Roll motion for Decay Test of the CALM Buoy using the DIC with Imetrum System at 62secs run*

The results of the experiment obtained is given in Figures 20-22. It can be seen that the motion response of the CALM buoy. It can be seen from the data in Figures 20-22 that the motion behaviour of the CALM buoy hose system was recorded during the experiment. The decay tests were also performed, and it depicts motion response for various motions performed across the run time of 62s. The surge response along the four (4) different reference points is consistent, but shows a different amplitude that is consistent, as the arrangement used was in a pattern that confirms that the results worked well as predicted and that good agreement from the surge can be used to validate similar numerical models, as shown in Figure 20-22. The first set of runs were completed in less than 62 seconds. The surge was strongest in reference 3 at 1,916m at 5.65s, as shown in Figure 20. The heave motion was similar for the 5 reference points acquired and was also maximum in reference 3 at 1,441m at 5.3s, as shown in Figure 21. The heave was likewise consistent for the 4 reference sites acquired, and was highest in reference 4 at 2.3 degrees at 5.4s, as shown in the roll motion in Figure 21. In Figure 22, the roll motion response for the 4 reference points are relatively close and have similar decay response, which shows that the motion of the buoy as presented in Section 3 have a good relationship.

It is noteworthy that this validation approach is conducted here using experimental modelling. It is also based on application by considering some models studied on existing theoretical marine hose models [96-100] and experimental hose models [147-150]. These models were compared to that of this present study and showed effective similarities in hose behaviour. In addition, the method of validation uses an application of existing

Orcaflex marine pipeline models for marine hoses validated using tension. This approach is similar to the studies conducted using Lazy-S configuration [24], Chinese-lantern configuration [146], and catenary S-lay marine pipes conducted with full-scale ocean tests [151]. Furthermore, deeper mechanism analysis was carried in addition to the current discussion, mainly focusing on the influence of certain parameters on the structural response. This includes studies on the shape effect, the methods for optimising the designs from the results obtained and using effective design suggestions. The consideration for the validation includes the key parameters investigated on the marine hoses, and the bending moment was selected. These considerations were conducted to confirm the model's validity.

### *2.12. The Coupling Method*

The coupling method was conducted in this research by using the hydrodynamic wave loads. This coupling approach used components of the numerical results by combined as *ANSYS AQWA+Orcaflex*. In this present study, the results of the comparative study between the coupled model and the uncoupled model for two submarine hoses (Hose1 and Hose2) under 0° flow angle are presented in Figure 23. The comparative study in Figure 23 shows that the 1st model case represents the uncoupled model while the 2nd model case represents the coupled model. The global loadings considered are the environmental data presented in Section 2.8. Comparisons were made between both models in the comparative study via numerical and statistical investigation. The result of the comparative study from the computation is given in Tables 14-16. It was recorded that the bending moment from the coupled model is 2.78 times greater than the uncoupled model. For each case of the coupled model, there was additional hydrodynamic RAO loads, which induced more responses in the bending moment, and hose curvature. The uncoupled model has a lower bending moment, and the average ratio from the statistical average ratio computed was found to be 0.53% for the bending moment component. From the comparisons on both component forces, it can be observed that both parameters considered agree well as it presents a uniform pattern for the three cases investigated.

**Table 14 Validation study using the bending moment of the submarine hose for Case1**

| Parameters | Bending Moment (KN.m) | | Average Ratio |
|---|---|---|---|
| | Uncoupled Model | Coupled Model | (Uncoupled/Coupled) |
| Hose1_Case1 | 117.6735 | 214.4112 | 0.54882161 |
| Hose2_Case1 | 136.5212 | 261.0225 | 0.523024643 |

**Table 15 Validation study using the bending moment of the submarine hose for Case2**

| Parameters | Bending Moment (KN.m) | | Average Ratio |
|---|---|---|---|
| | Uncoupled Model | Coupled Model | (Uncoupled/Coupled) |
| Hose1_Case2 | 87.54206 | 188.5113 | 0.464386273 |
| Hose2_Case2 | 93.11749 | 298.8106 | 0.311627131 |

632

633

**Table 16 Validation study using the bending moment of the submarine hose for Case3** 634

| Parameters | Bending Moment (KN.m) | | Average Ratio (Uncoupled/Coupled) |
|---|---|---|---|
| | Uncoupled Model | Coupled Model | |
| Hose1_Case3 | 153.9478 | 270.7054 | 0.568691278 |
| Hose2_Case3 | 137.3706 | 379.3597 | 0.362111737 |

635

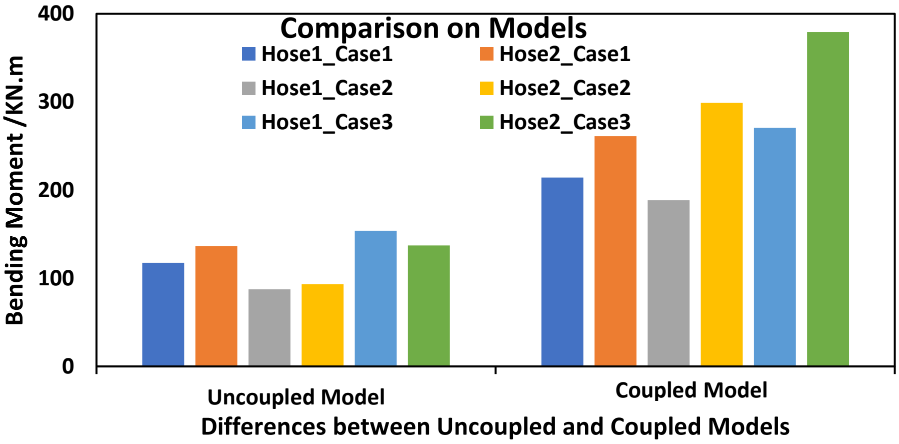


636

*Figure 23 Comparative study using the bending moment of the submarine hose comparing the uncoupled and coupled models* 637

638

639

## *2.13. Dynamic Amplification Factor (DAF)* 640

The comparison on computations led to the additional investigation on the response behaviour based on design factors and guidance values that could be generated from this study. Parametric studies conducted on the hoses included the bending moment, effective tension and hose curvature. DAF investigations were also performed on these hose parameters investigated. The dynamic amplitude factor or dynamic amplification factor (DAF) is depicted simply as the response factor for the dynamic response amplitude versus the static response amplitude. In that respect, the relationship for the Dynamic Amplification Factor of hose ($DAF_{hose}$) is given in Equation (23). The static response amplitude is the response amplitude operator obtained during static analysis. More fundamental studies on DAF are available in the literature [152,153]. 641–650

651

$$DAF_{Hose} = \frac{Dynamic\ Response\ Amplitude\ (coupled\ hose\ model\ having\ hydrodynamic\ loads)}{Static\ Response\ Amplitude\ (uncoupled\ hose\ model\ lacking\ hydrodynamic\ loads)} \quad (23)$$ 652

653

In real environmental ocean conditions, accurate prediction of the amplitude motion of the offshore structure must be performed before any offshore operation is carried out, as specified in design guidelines. This first design analysis is conducted initially in the 654–656 static stage. Based on the DAF studies, some DAF values were recommended for the submarine hoses, however relative to the submarine hose position on the seabed.

### 2.14. Analysis Method

The analysis method is based on different case studies investigated, and coupled and uncounpled models. In addition, the effect of the hydrodynamic loads, the effect of current on buoy motion, the response from the RAOs, the response from the first order wave forces, the $DAF_{hose}$ effects and WCI studies were all conducted as stated in Section 3 and 4.

## 3. Results and Discussion

In this section, the results from the numerical studies on the motion response of the CALM buoy are presented. The results from the sensitivity studies include some parametric studies obtained from the numerical studies. The influence of hydrodynamic loads on CALM buoy submarine hoses has been observed to have an influence on the hose-string curvature, effective tension, and the bending moment.

### 3.1. Results of hydrodynamic studies

The results of the hydrodynamic studies are presented in this section.

#### 3.1.1. Results of Coupled and Uncoupled Model

The studies on the coupled and the uncoupled models were conducted in this section. The bending moment profile showing Hose1, Hose2, 3 sea states and 5 wave angles utilized in the uncoupled model is shown in Figure 24, while that for the coupled model is shown in Figure 25. From Figure 24, it can be observed that different wave angles reflect a different profile on the bending moment without added RAO wave loads. However, they are closely related. The $0^0$ wave angle has the highest profile among these five cases looked at. It shows that at $0^0$ incidences, the bending moment per hose case is higher than that of $30^0$, $60^0$, $90^0$, and $120^0$ incidences. Also, the Hose1_Case2 and Hose2_Case2 have the highest distribution of 153.95kN and 137.37kN, respectively. This implies that the extreme environmental loadings directly impact the hydrodynamic characteristics of the submarine hoses. It can also be seen that the least hose cases are the $90^0$ hoses in Case1 and Case2 but not in Case3, which implies that at higher environmental loadings, the hose wave incidence at right angles will induce higher diffraction on the hose. Thus, it will react by presenting the higher response due to the shape of the hose and the wave-current interaction that it undergoes at that time period. It implies that there are highly sensitive responses from higher time periods by the hoses. In Figure 25, it was recorded that the coupled model (having the addition of hydrodynamic RAO wave loads) had higher distributions compared to the uncoupled model (without addition of hydrodynamic wave loads) in Figure 24. The results in Figure 25 show that at $0^0$ incidences, the bending moment per hose case is higher than that of $30^0$, $60^0$, $90^0$ and $120^0$ incidences. Also, the Hose1_Case2 and Hose2_Case2 have the highest distribution of 270.71kN and 379.36kN, respectively. Next to the $0^0$ cases are the $30^0$ cases, which showed a closer profile related to the $0^0$ cases. However, it can be observed that the hose bending moments at Case3 in Hose1_Case3 for $30^0$ (360.01kN) is higher than the hose bending moments at Case3 in Hose1_Case3 for $0^0$ (270.71kN). This implies that the higher time period also has an effect on the hose at that wave angle. A similar higher profile is observed in $120^0$, which is about a quadrat turn through of $30^0$ incidence. The comparison between the uncoupled and the coupled models in Figures 24 and 25, respectively, shows that the coupled models generally have higher bending moment than the uncoupled models.

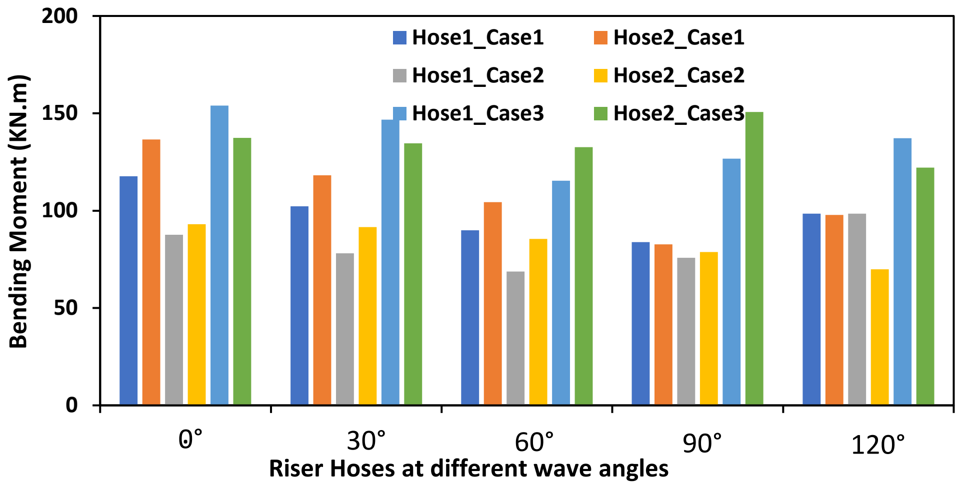


*Figure 24 Bending moment profile for uncoupled model showing Hose1, Hose2, 3 sea states and 5 wave angles utilised*

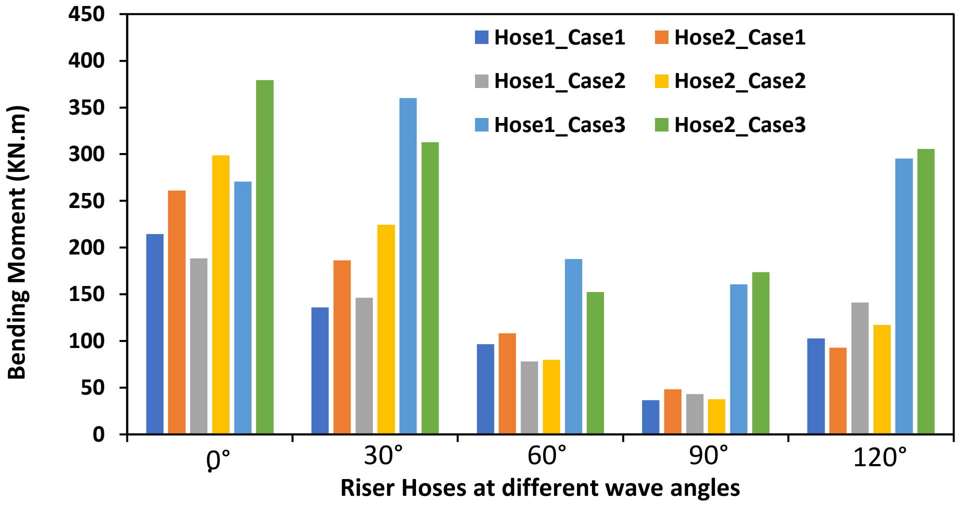


*Figure 25 Bending moment profile for coupled model showing Hose1, Hose2, 3 sea states and 5 wave angles utilised*

#### 3.1.2. **Results of Hose Curvature Sensitivity**

The curvature profiles for the marine hose under Lazy-S and Chinese-lantern configurations are presented in Figure 26(a-d). It shows the cases 'including loadings from hydrodynamics' and 'excluding loadings from hydrodynamics' are respectively. Some deformations were observed in the hose, which occurred where the MBR is high. Similarly, some curvature distributions are observed from the behaviour of the submarine hoses via dynamic analysis. As observed in Figure 26(a-d), the 0° flow angle models have the highest curvature via arc length of the hose in both configurations. However, the 90° flow angle models reflected minimal curvature via the arc length of the hose. Damping is one method to minimise hose curvatures, in addition to the inclusion of the hydrodynamic loads. It was also observed that the hoses subjected to cross-flow directions in the cases for 0° in both Lazy-S and Chinese-lantern configurations presented greater curvatures which further developed on inclusion of the hydrodynamic loads. In comparing the models for Lazy-S and Chinese-lantern configurations, while the curvature plot in the Lazy-S cases sag, that in the Chinese-lantern cases are hugging. Also, the curvature profiles for the Lazy-S configurations have higher curvatures at the top connections, which can be attributed to the weight from the longer length of the hose-string at its connection point to the manifold on the CALM buoy.

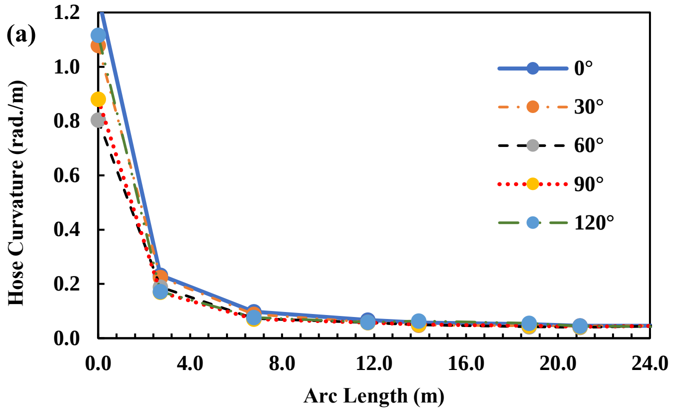


(a) Hose Curvature including hose hydrodynamic load in Lazy-S config.

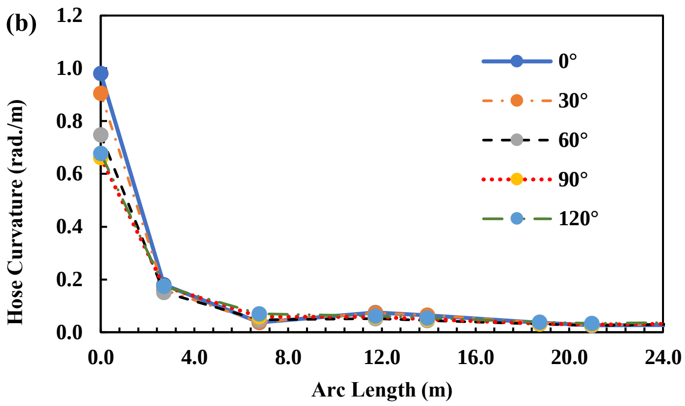


(b) Hose Curvature excluding hose hydrodynamic load in Lazy-S config.

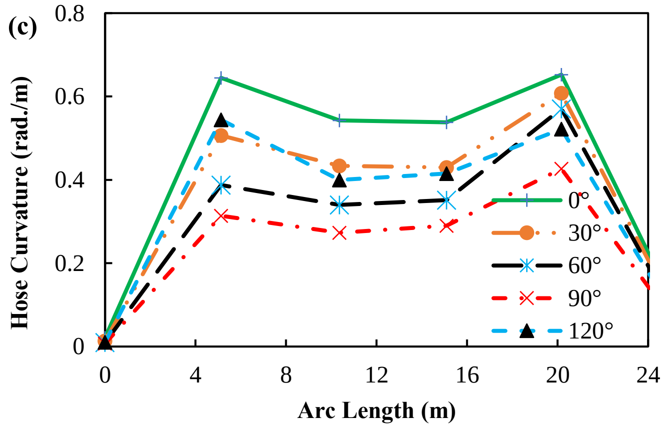


(c) Hose Curvature including hose hydrodynamic load in Chinese-lantern config.

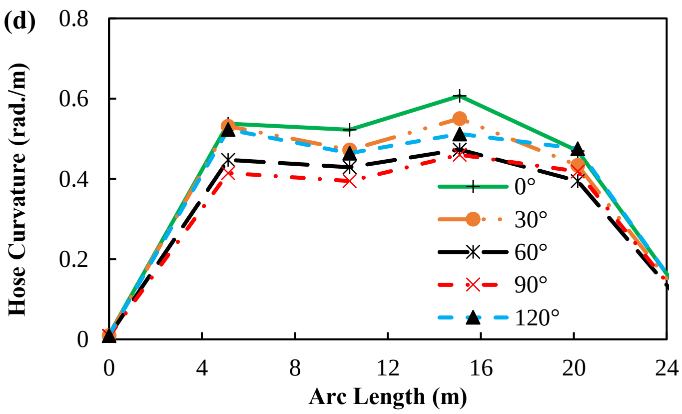


(d) Hose Curvature excluding hose hydrodynamic load in Chinese-lantern config.

***Figure 26 Influence of loadings from hydrodynamics on the curvature of the submarine hose***

#### 3.1.3. **Results of Hose Effective Tension Sensitivity**

The effective tension profiles for the marine hose under Lazy-S and Chinese-lantern configurations are presented in Figures 27(a-d). It shows the cases 'including the loadings from hydrodynamics' and 'excluding the loadings from hydrodynamics', respectively. The tension profiles present a steady distribution running through the arc length of the hoses. However, the comparative studies on both configurations show higher distributions recorded in the Lazy-S case than the Chinese-lantern case, but the Chinese-lantern case has more fluctuations than the Lazy-S case. This is attributed to the result of bending in response to waves and currents. The distribution recorded on the effective tension profile is not undulating or fluctuating like the bending moment profiles presented in Figure 28. The reason is that hose tensions are not always a function of the flexural stiffness, but due to nonlinearities in the hose material properties. It was also observed that the cross-flow model cases, particularly the case 0° exhibited greater tensions in comparison to the case 90°. Thus, it can be deduced that an increase in the effective tension can be induced by increasing the hydromantic loads of the hose. In addition, the points of attachment of the hoses to the PLEM and to the manifold underneath the CALM buoy exhibited maximum effective tensions of high magnitudes. Thus, the angle of inclination of design for the manifold is recommended to be at about 30°, as this manifold angle enhanced better results, but it is also subject to the manufacturer's choice, the environmental conditions and the marine hose properties. Lastly, the hose-string recorded the highest flexural and axial stiffness resulting from the end restrictions, but other relatively flexible sections. More flexible hose sections with less bending moments may be used to withstand hydrodynamic loadings, and the float type for the hoselines used may require more inertia properties.

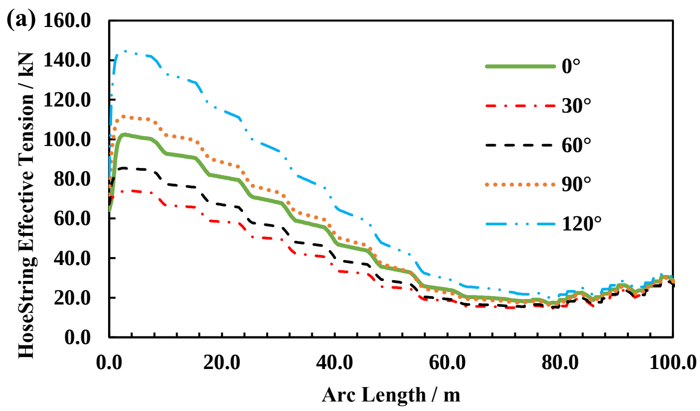


(a) Coupled Hose Effective Tension in Lazy-S config.

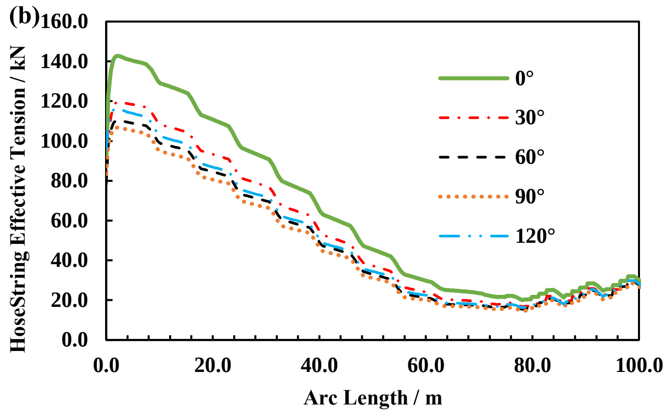


(b) Uncoupled Hose Effective Tension in Lazy-S config.

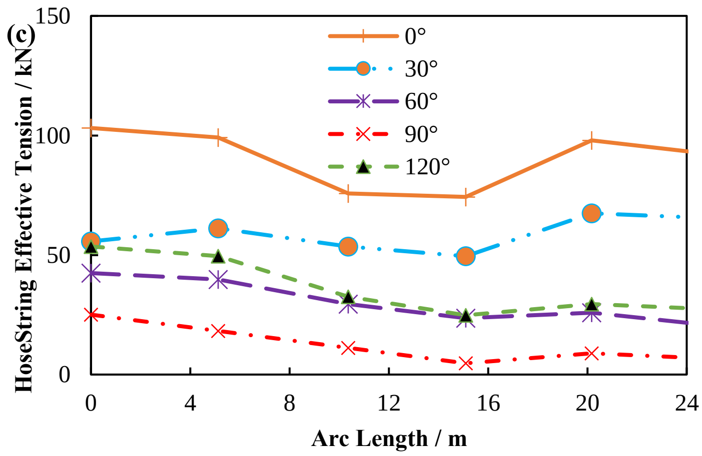


(c) Coupled Hose Effective Tension in Chinese-lantern config.

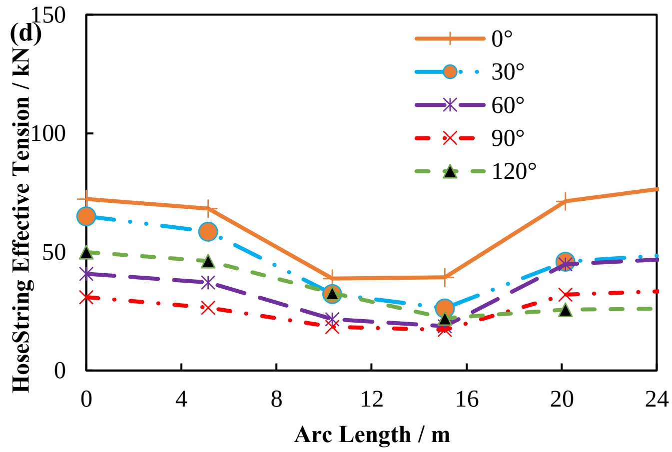


(d) Uncoupled Hose Effective Tension in Chinese-lantern config.

***Figure 27 Influence of loadings from hydrodynamics on the effective tension of the submarine hose***

#### 3.1.4. **Results of Hose Bending Moment Sensitivity**

The sensitivity of hose bending moment was also investigated in this research. As observed in Figure 28, the hose curvature from the bending moment sensitivity is within the design limit as stipulated in OCIMF (2009). Wave and current loads, as well as other hydrodynamic loads, induce the hose curvature. The bending moment profiles for the marine hose under Lazy-S and Chinese-lantern configurations are presented in Figures 29(a-d). It respectively shows the cases 'including the loadings from hydrodynamics' and 'excluding the loadings from hydrodynamics'. As is evident in Figure 29(c-d), significantly greater bending moments are recorded at both ends of the marine hose. However, the bending moments for the arc length located within the middle and in-between end sections have minimal bending moments recorded. The bending moment profiles were recorded at the two ends of the marine hoses under the cases 'including the hose hydrodynamic loads'. However, for the hose sections that lie in-between, significantly larger moments, with the exception of the case 90°. The bending moment behaviour resulted from the twisting of the hose. From the comparative studies on Lazy-S and Chinese lantern cases, more undulations are observed in the lazy-S cases than the Chinese-lantern cases due to the longer length of the submarine hoses and the floats attached on the submarine hose-string in the Lazy-S configuration. During twisting, the hose deformations were observed to also be a function of the wave and the buoy rotations. Thus, larger moments from the twisting induced at the case 90° for the Lazy-S configuration are different from that of the Chinese-lantern configuration. In terms of energy dissipation, higher energy magnitudes are released during twisting than during bending. This, in turn, results in relatively lesser stiffness of the buoy on the system

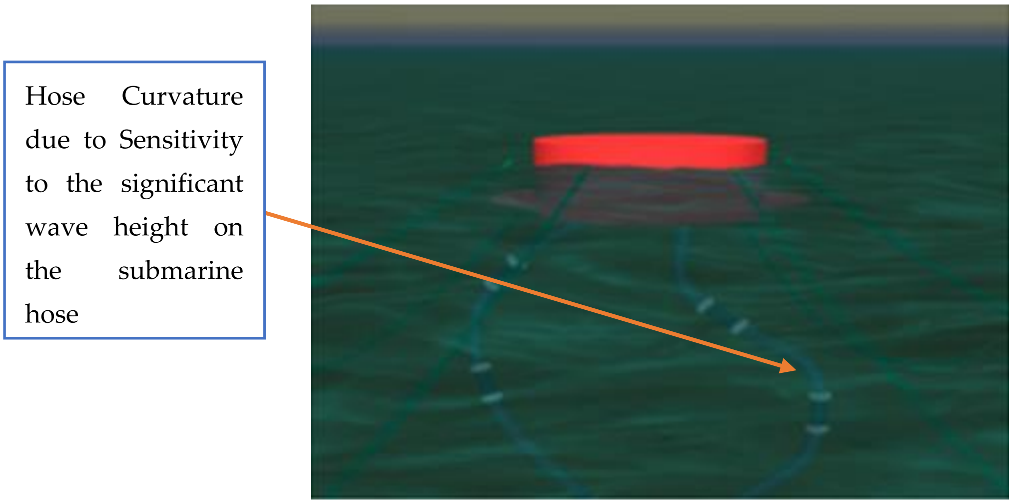


*Figure 28 Curvature profile of submarine hose using Chinese-lantern configuration*

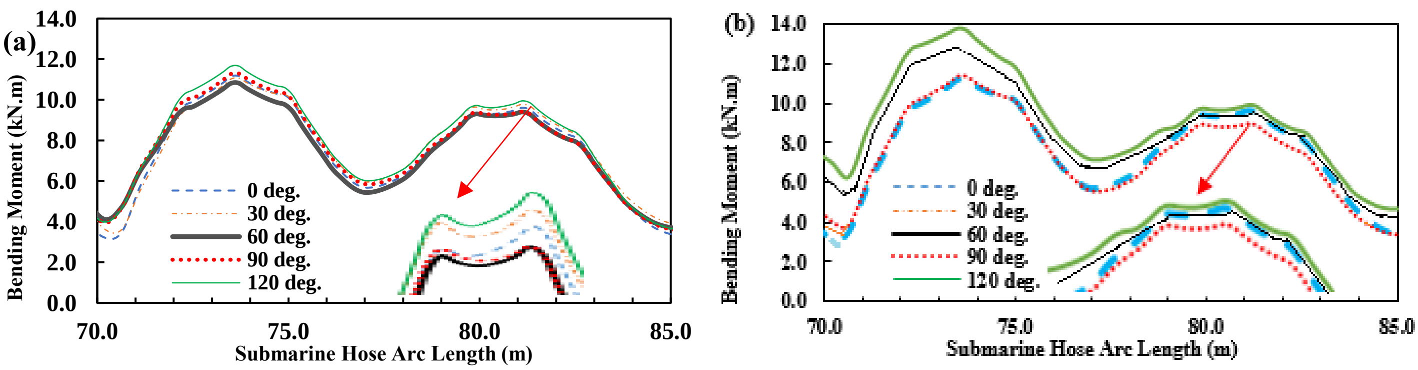

(a) Coupled model for Hose Bending moment in Lazy-S config.

(b) Uncoupled Hose Bending moment in Lazy-S config.

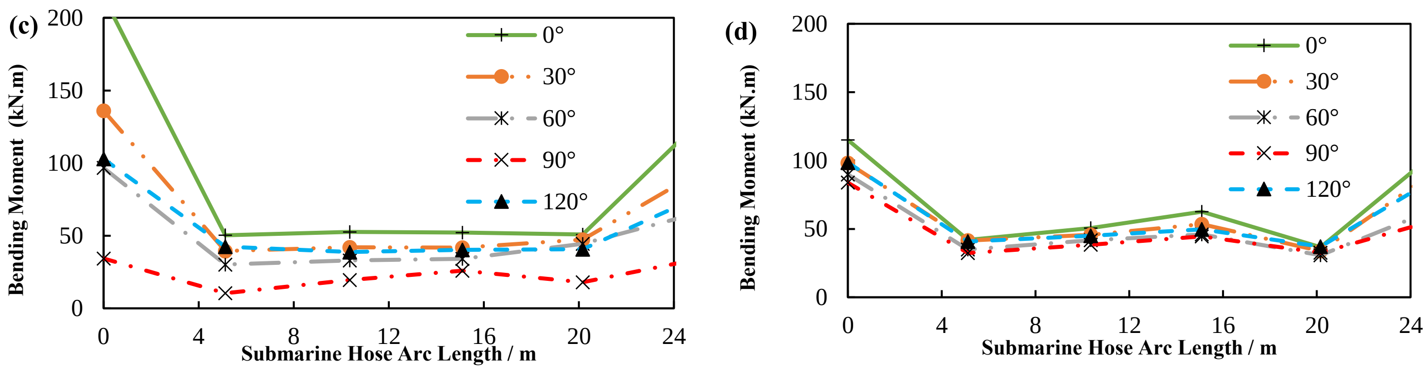


(c) Coupled Hose Bending moment in Chinese-lantern config.

(d) Uncoupled Hose Bending moment in Chinese-lantern config.

***Figure 29 Influence of hydrodynamic loads on the bending moment of the submarine hose***

#### 3.1.5. **Results of DAF of hose ($DAF_{hose}$) Sensitivity**

The sensitivity studies on the $DAF_{Hose}$ for marine hoses are calculated by considering one submarine hose-string, Hose1 as presented in Figure 30(a-f). The comparisons of the curvature profiles for Lazy-S and Chinese-lantern configurations showing the cases including the hydrodynamic loads and excluding the hydrodynamic loads are shown in Figure 30(a-b) by the curvature $DAF_{Hose}$. The behaviour of submarine hoses is subject to the buoyancy of the hose and the attached floats. However, with some flexibility in the hose-string under waves and current loadings, the hose string is also designed to resist such forces and moments, resulting in high curvatures. As a result, the floats are positioned at strategic positions; however, the locations with maximum bending require additional reinforcements. In the Lazy-S configuration in Figure 30(a), high curvature profiles are observed in 0°, similar to the result obtained during accidental operation (disconnection), which presents the most threatening scenario. However, the average hose curvature $DAF_{Hose}$ is not that high. At worst cases of hose disconnection, the $DAF_{Hose}$ could have such high values of 2.5. However, the guidance value of 1.5-2.0 for curvature $DAF_{Hose}$ is advised here, as seen in Figure 30(b) for the normal operation under Chinese-lantern configuration. In Figure 30(c-d), the profiles of effective tension $DAF_{Hose}$ on the submarine arc length. The presented analyses suggest a guidance value of 1.0 - 2.0 for effective tension $DAF_{Hose}$ and bending moment $DAF_{Hose}$. In offshore field practice, determination of significant tensions are at the touch down zone (TDZ), and connection to PLEM and at Buoy manifold. This might be as a result of higher responses from the wave frequency motion, affected by damping, induced by the wave drift, and perturbed by the seabed parameters. As such, the effective tension may be uniformly distributed along the hose arc length but varying bending moment. This behaviour is also due to the effect of the hydrodynamic coefficients of the buoyancy floats on the hose body. From the DAF curves, it can be observed that the connections had the highest bending moments. This can be attributed to some drag occurrence on the floating buoy. In principle, there is viscous drag resulting from friction between the surface of the buoy's body and the fluid particles. Thus, reducing both the coefficient of drag and the coefficient of damping is one method that is recommended to offset this phenomenon. Another method is to increase the reinforcement along such locations of high bending. The $DAF_{Hose}$ for the bending moment distributions throughout the hose for Lazy-S and Chinese-lantern configurations is presented in Figure 30(e-f). It shows the cases 'including hydrodynamic loads' and 'excluding hydrodynamic loads' on the hose's arc length. In similar fashion, the design recommendation for the bending moment $DAF_{Hose}$ is a guidance value of 2.0. It is also recommended that accidental conditions are investigated in further studies based on hose disconnections, to predict the structural effect on the structure's integrity and ascertain safety guidelines for improving operations on CALM buoy-hose systems.

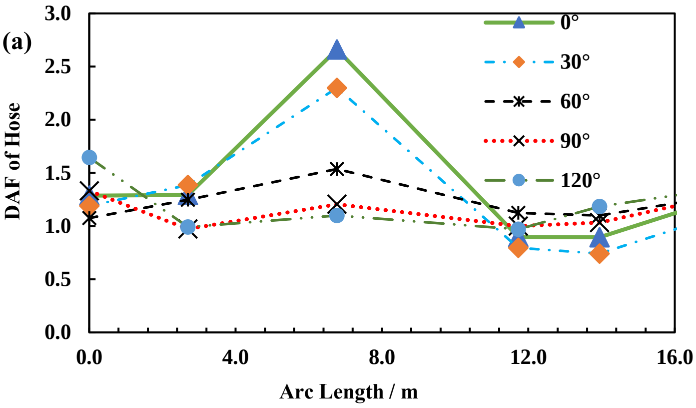


(a) Curvature $DAF_{Hose}$ for Hose in Lazy-S config.

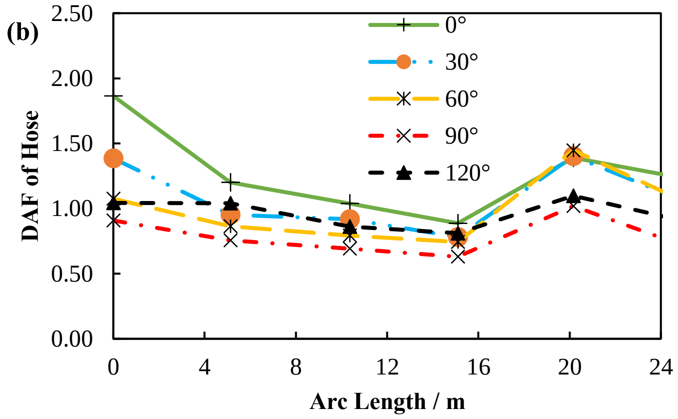


(b) Curvature $DAF_{Hose}$ for Hose in Chinese-lantern config.

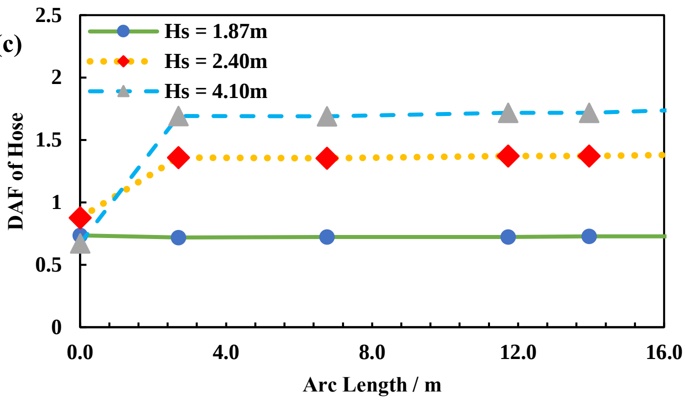


(c) Effective Tension $DAF_{Hose}$ for Hose in Lasy-S config.

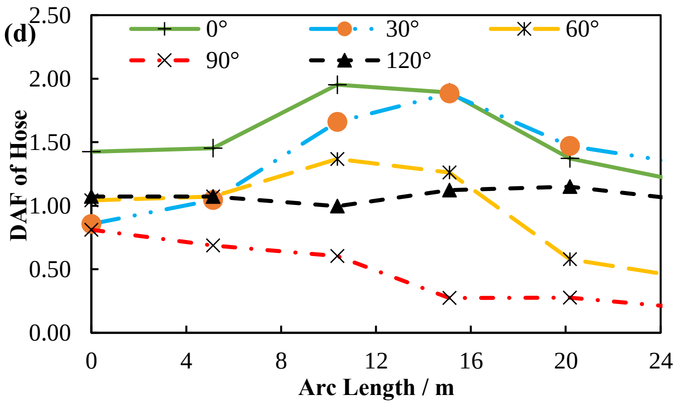


(d) Effective Tension $DAF_{Hose}$ for Hose in Chinese-lantern config.

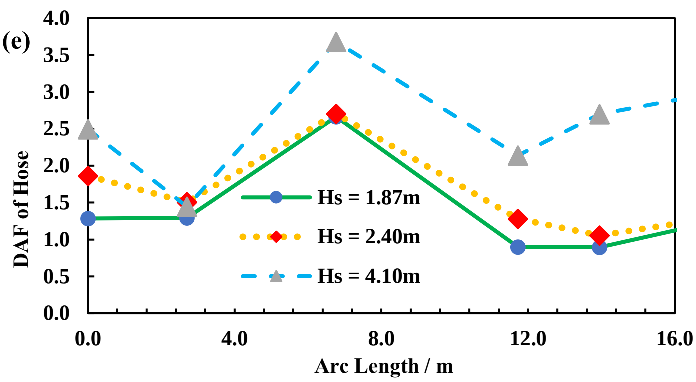


(e) Bending moment $DAF_{Hose}$ for Hose in Lazy-S config.

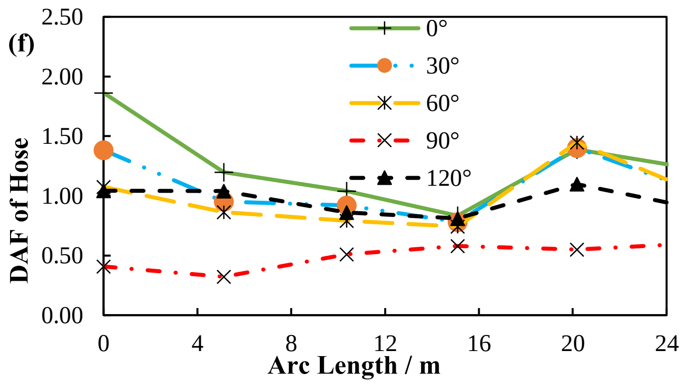


(f) Bending Moment $DAF_{Hose}$ for Hose in Chinese-lantern config.

***Figure 30 Influence of loadings from hydrodynamics on the $DAF_{Hose}$ of the submarine hose***

### *3.2. Results of wave-current interactions*

The results of the wave-current interaction studies are presented in this section.

#### 3.2.1. **Results of Current on buoy motion RAOs (Response Amplitude Operators)**

The effect of current velocity on the CALM buoy motion RAOs have been presented in this section. From the literature review, the effect of current velocity on the wave forces acting on the CALM buoy motion has not been previously presented in any literature. Still, there are exiting works on other floating structures like semisubmersibles [55-58,154]. It should be noted that the CALM buoy has 6DoFs. However, the results of the surge, heave, pitch, and yaw presented in Figure 31 are to show the influence of wave-current interaction and the effect of current velocity on the floating buoy. This investigation was conducted using three current profiles: 0.5m/s, 1.0m/s and 1.5m/s. The RAOs were obtained under irregular waves using the environmental condition for extreme cases. It was recorded in Figure 31(a) that the higher the current velocity, the lower the surge profile. However, Figure 31(b-d) recorded that the higher the current velocity, the higher the heave, pitch and yaw profiles. This shows that there is a variation in the effect of current velocity from different motion characteristics. Thus, recommendations include that CALM buoy hose systems should be well monitored using real-time monitoring systems like Offshore Monitoring Systems (OMS), Buoy Monitoring Systems (BMS) and Hose Monitoring Systems (HMS). Secondly, findings on the CALM buoy motion are with respect to the environmental conditions, and not representative of all sea conditions. However, the CALM buoys respond to both regular and irregular waves, as well as currents depending on its collinearity.

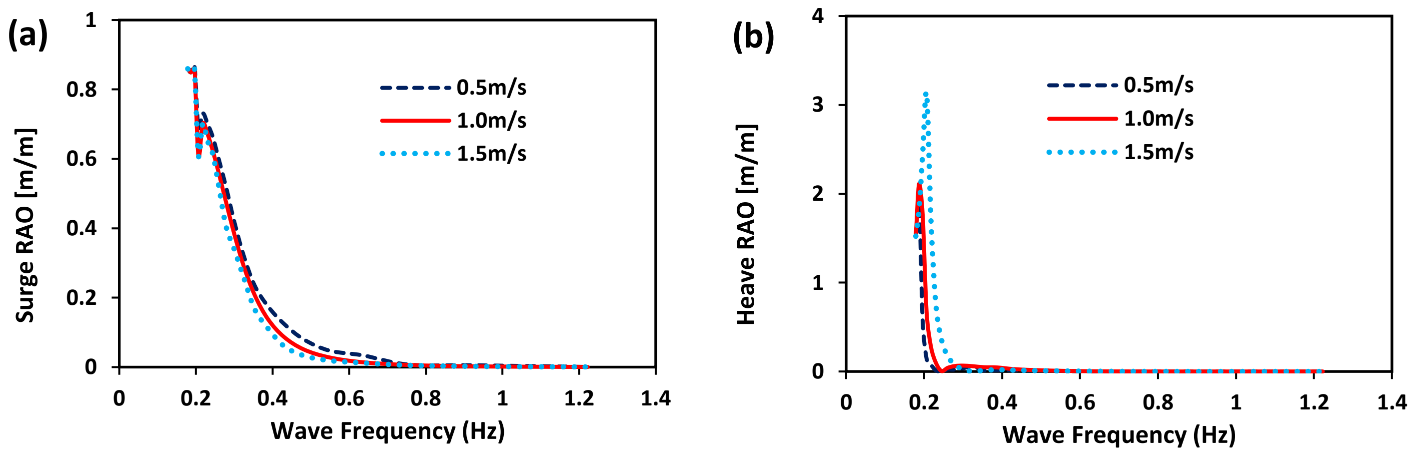

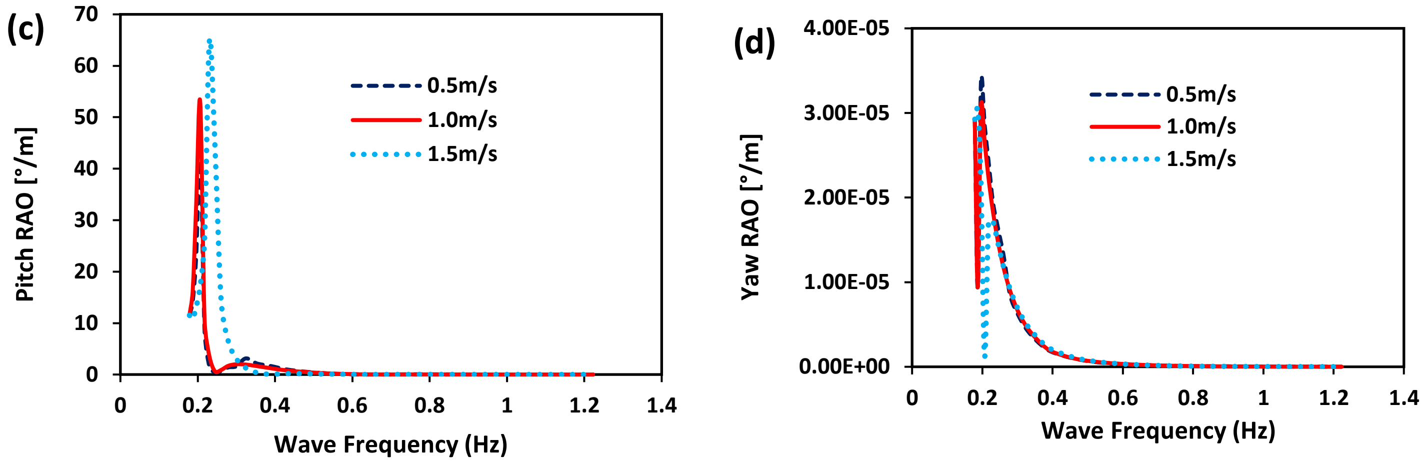


***Figure 31 Influence of current velocity on the motion RAOs for the CALM buoy, showing (a) surge, (b) heave, (c) pitch and (d) yaw***

3.2.2. **Results of Current on first order wave forces from CALM buoy motion**

The effect of current velocity on the CALM buoy motion RAOs have been presented in this section. From Figure 32, it can be observed that the current has some effect on first-order wave forces for the different motions of the CALM buoy. This investigation was conducted using three current profiles: 0.5m/s, 1.0m/s and 1.5m/s. The first-order wave forces were obtained under irregular waves using the environmental condition for extreme cases. It was recorded in Figure 32(a) that the higher the current velocity, the lower the surge profile. Contrary to this, in Figure 32(b), the higher the current velocity, the higher the heave profile. In Figure 32(c-d), the higher the current velocity, the less the pitch profile and the less the yaw profile, respectively. This shows that the current velocity has a direct relationship with the motion behaviour. This makes some contribution to its hydrodynamic characteristics but requires further study on that.

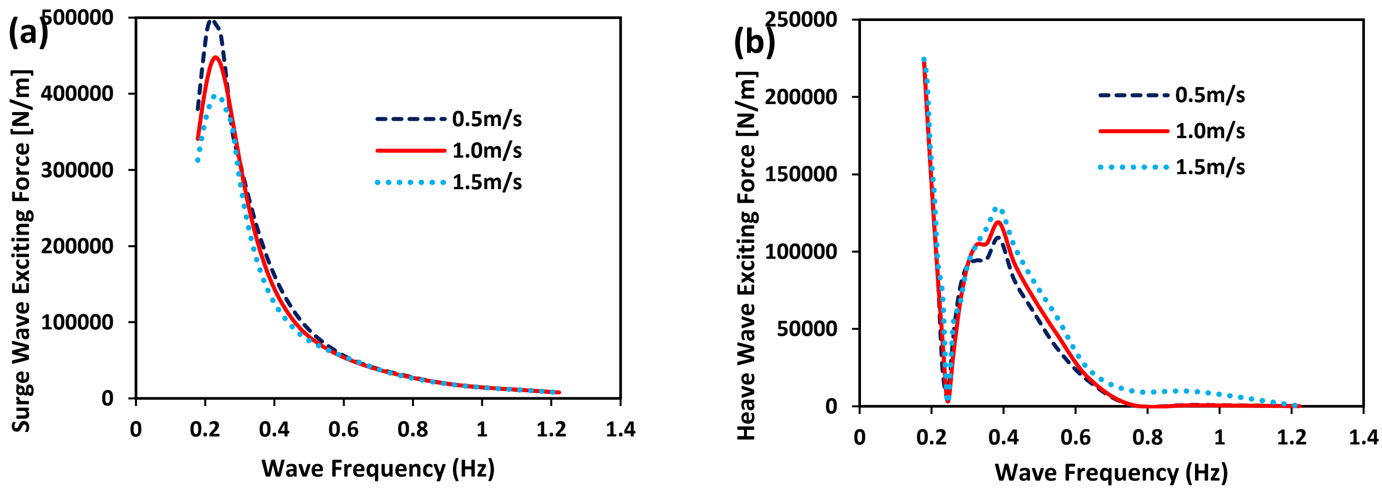

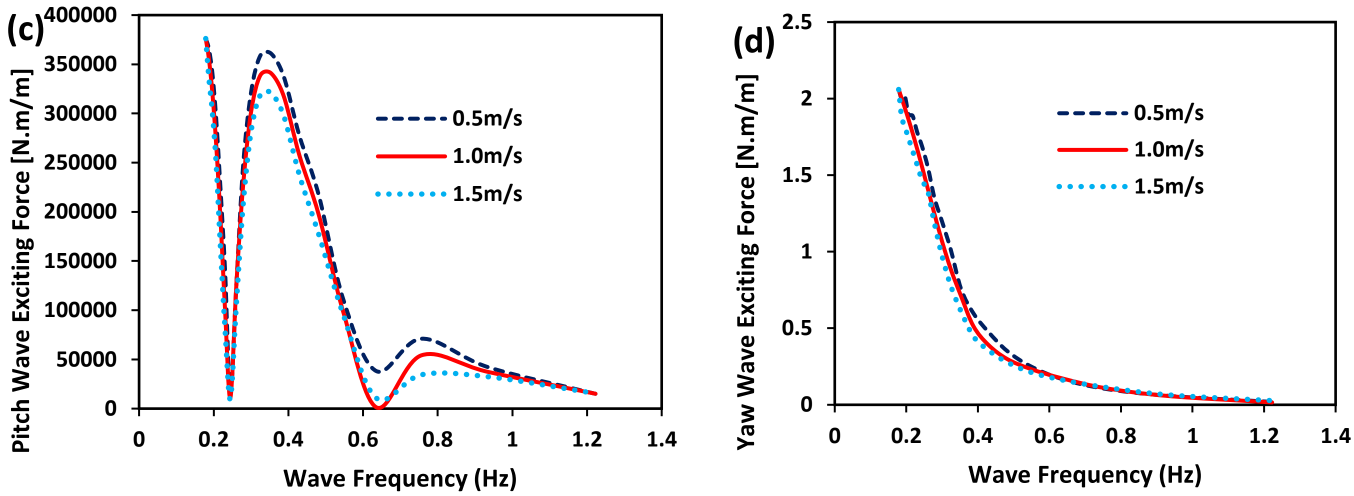


***Figure 32 Influence of current velocity on the first order forces for the CALM buoy, showing (a) surge, (b) heave, (c) pitch and (d) yaw***

The motion response is also a function of the ocean current, azimuthal direction, system acceleration, system velocity, and the relative position of the attached hoses and mooring lines. The first order wave forces on this system for the three (3) different current velocities present similarities in form and profile. Also, they have different peaks on the surge, heave, pitch, and yaw but at the same natural frequency range for the system. The effect of the current velocity on the yaw motion is least or almost negligible, as observed in Figure 32(d). However, due to the resonating frequency, the effect of the current velocity is relative to the motion- if translational like surge and heave, or rotational like pitch and yaw. In the case of the heave, the frequency profile is higher from 0.299Hz to 1.223Hz, unlike in the surge motion, where the frequency profile is 0.179Hz to 0.278Hz. This behaviour shows a relationship between first-order wave forces and the three (3) current velocities investigated. However, further investigation is also recommended by considering the effect of CALM buoys with different draft sizes. Based on studies on Boundary Element Methods [155-158], waves and currents impact floating bodies. These earlier studies found that wave energy is absorbed, including elevated bodies and deformable bodies. Unlike the submarine hose, the CALM buoy is considered an elevated body that floats on the surface of the sea, across its draft line. This study also shows a variation in the effect of current velocity from different motion characteristics.

#### 3.2.3. **Results of Seabed Current and Surface Current Sensitivity on hose**

The sensitivity of current was investigated for both the seabed current and surface current on the nonlinear seabed model in Lazy-S configuration. The surface current velocity has an eminent function in designing CALM buoy systems for loading and offloading operations. To investigate its influence, some surface current values are used; for 0.45 m/s, 0.65 m/s, 0.75 m/s, 0.9 m/s, and 1.0 m/s. As the surface current velocity increases, the bending radius (curvature) decreases, the bending moment decreases as well as an increase in the effective tension, as in Figure 33(a-b). Considering the seabed currents, the seabed current velocity parameters considered are as follows: 0.35 m/s, 0.45 m/s, 0.75 m/s and 0.9 m/s. For the same surface current velocity, an increment on the seabed current velocity has corresponding reduced effective tension and reduced bending moment, as shown in Figure 33(c-d). An increase in seabed current velocity reduces bending radius (curvature) and increases effective tension, and bending moment.

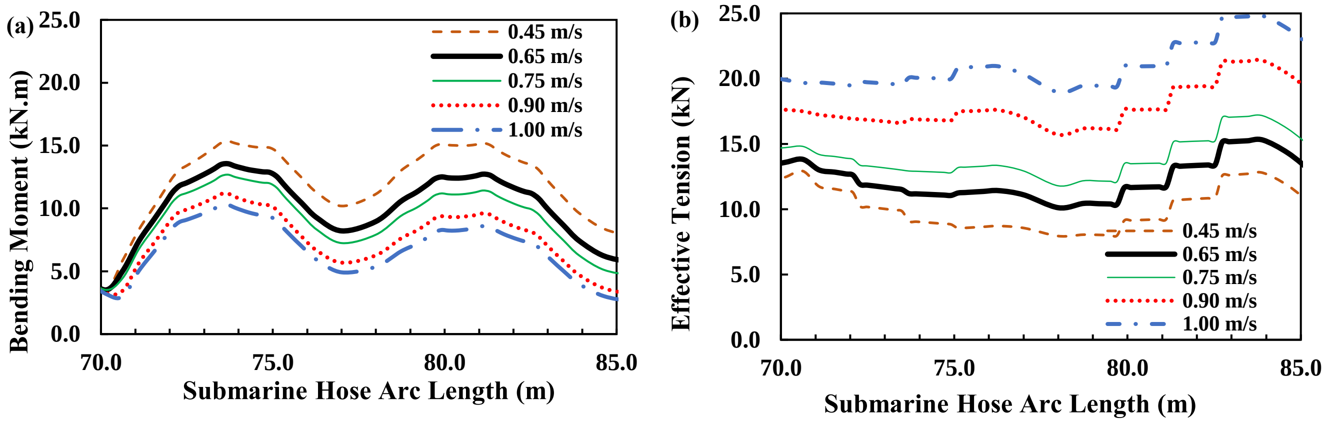


(a) Bending Moment for surface current on arc lengths (b) Effective tension for surface current on arc lengths

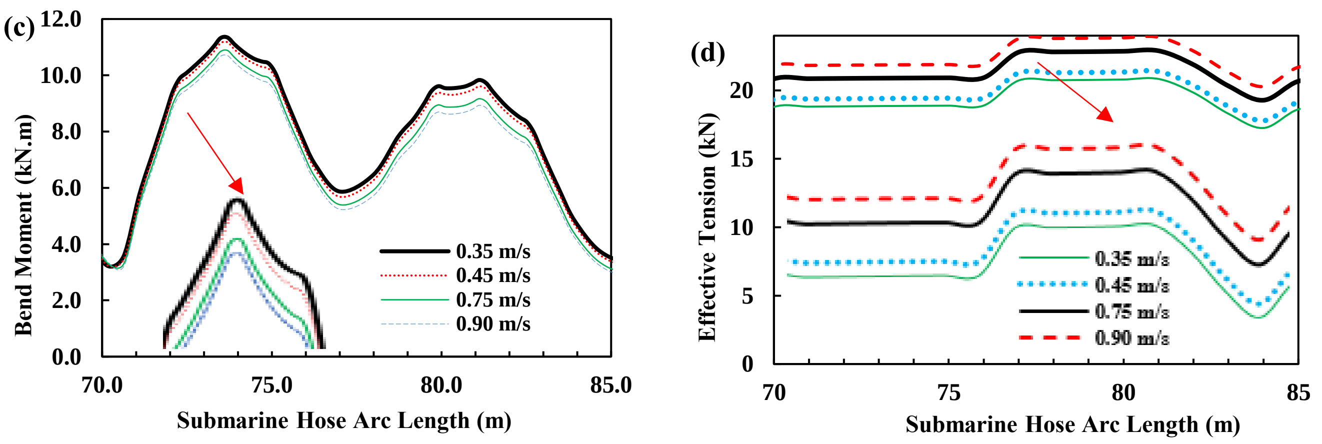


(c) Bending Moment for seabed current on arc lengths (d) Effective tension for seabed current on arc lengths

***Figure 33 Influence of surface currents (a,b) and seabed currents (c,d) on submarine hoses***

3.2.4. **Results of Current Attack Angle Sensitivity on marine hose**

The sensitivity of the current attack angle investigated on the submarine hoses in Lazy-S configuration was investigated for the following: $60^0$, $90^0$, $120^0$, $150^0$, and $180^0$, as presented in Figures 34. It shows that the current attack on the hose-string was highest at $60^0$ close to the TDZ. Similarly, the $60^0$ hose had highest effective tension at the top of the submarine hose at 123.91 kN but had lowest tension of 3.52 kN at TDZ. Due to the non-linear seabed profile, the effective tension may have constant distribution along the hose arc length, but varying bending moment. This is due to the effect of the buoyancy hose on the hoses. However, the $60^0$ model had least curvature at the top of the submarine hose. Thus, finite element studies on marine hose models are recommended to investigate the mechanical behaviour, as seen in [159-164].

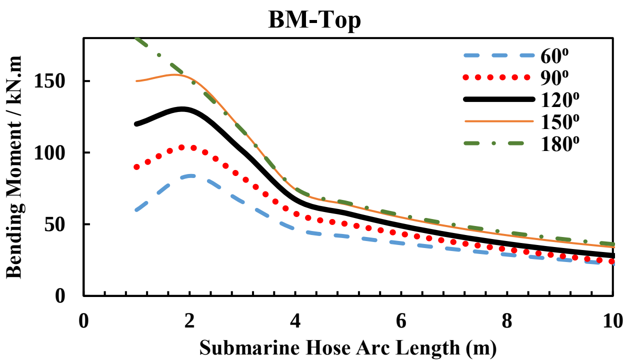


(a) Bending Moment for current attack angle at hose top

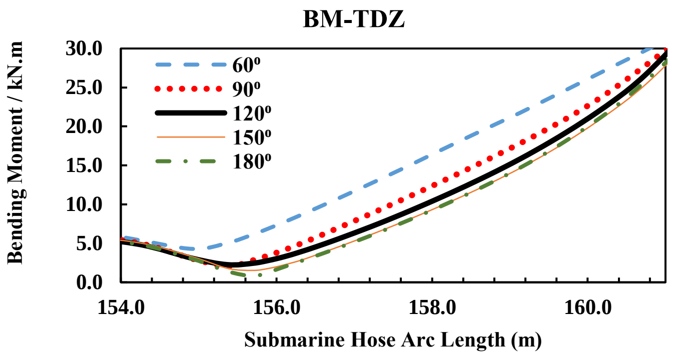


(b) Bending Moment for current attack angle near PLEM

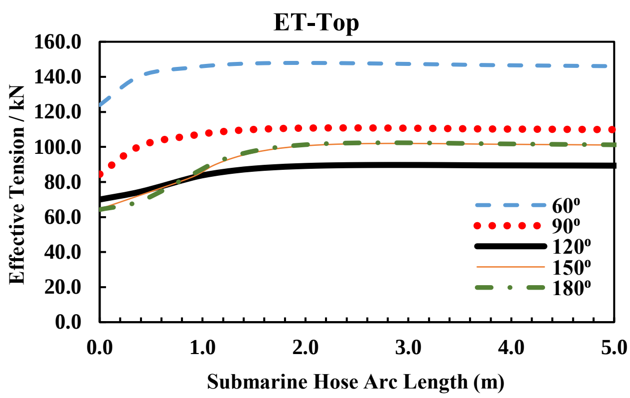


(c) Effective tension for current attack angle

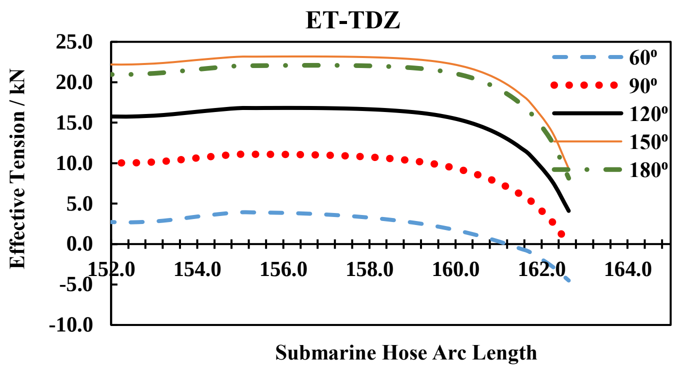


(d) Effective tension for current attack angle near PLEM

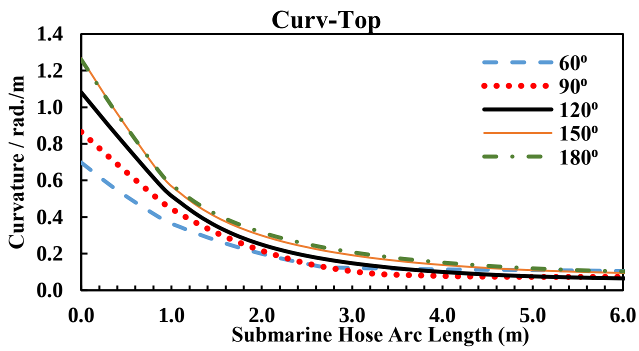


(e) Curvature for current attack angle

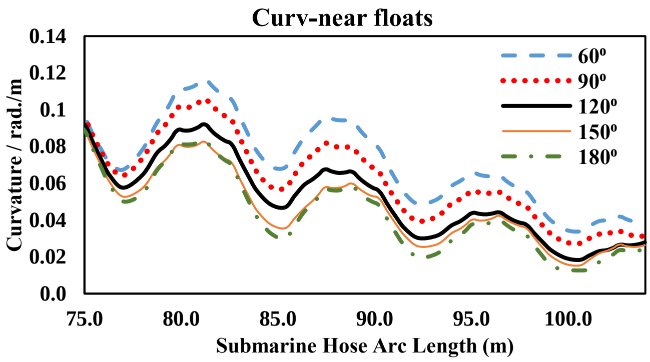


(f) Curvature for current attack angle near hose floats

***Figure 34 Influence of surface currents (a,b) and seabed currents (c,d) on submarine hoses***

### 3.2.5. **Results of Time Response Sensitivity for the CALM buoy system**

The extent of the values largely depended on flow angle. A series of snapshots from the simulation in Orcaflex for Chinese-lantern configuration at 0° flow angle at $H_s$=1.87m, $T_z$=4.10s and $T_P$=5.27s is presented in Figure 35. It depicts the time response on the hose curvature behaviour, as observed at different times as recorded. It can be observed that the hose has snaking behaviour with the highest curvature observed at time t=2,998s. As such, it is recommended to increase the reinforcement at such locations.

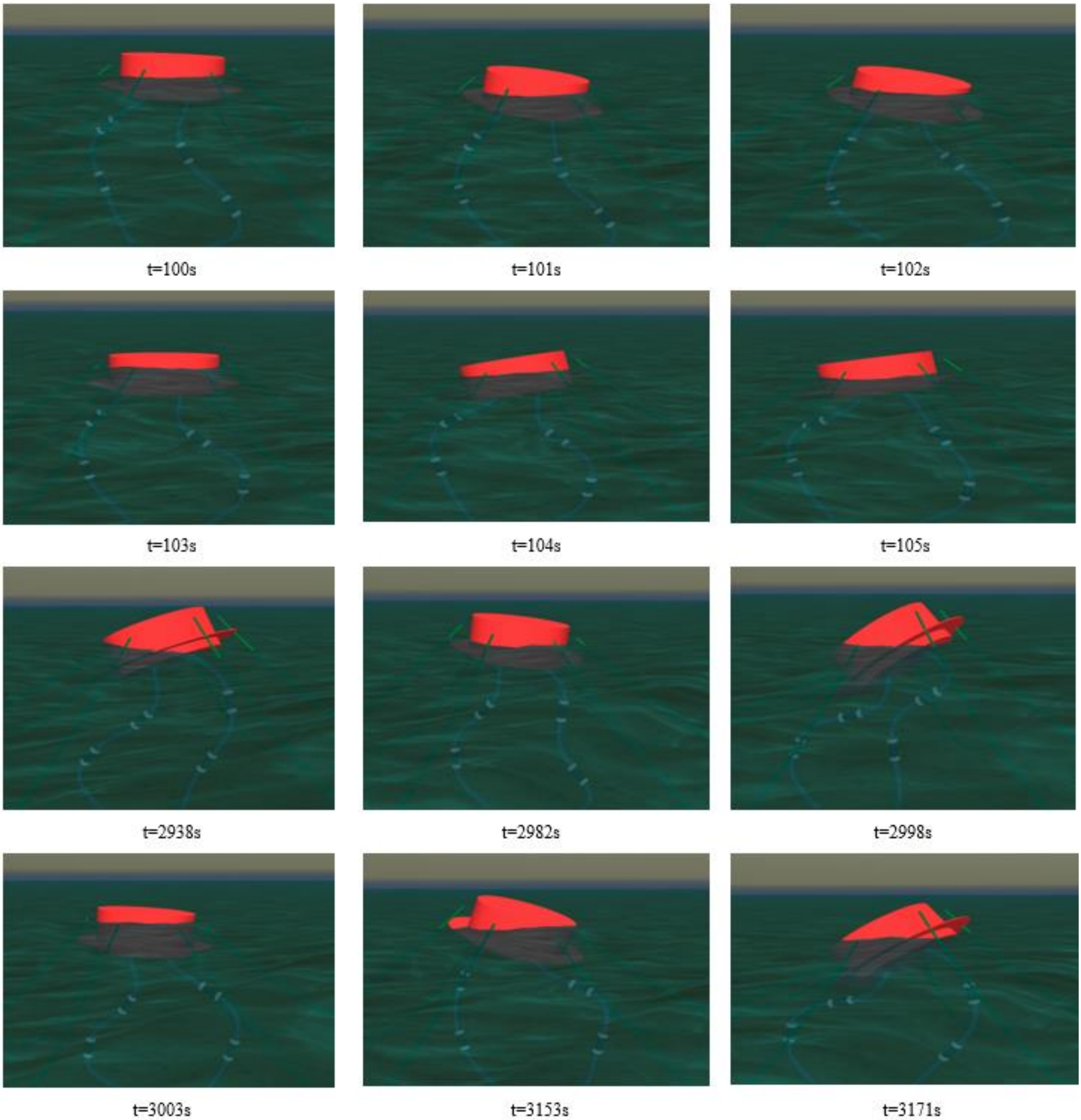


**Figure 35 Snapshots of hose behaviour at different times observed, Hs=1.87m, Tz=4.10s, 0° flow angle**

## 4. Further Discussion

Detailed numerical investigation on CALM buoys with submarine hoses was carried out in two configurations: Lazy-S and Chinese-lantern. It was designed under irregular waves for a cylindrical CALM buoy. The hydrodynamic panel was developed in ANSYS AQWA and solved using diffraction theory and JONSWAP Wave Spectrum for the three (3) environmental conditions used. The boundary conditions considered for the submarine hoses were attached on the PLEM and hose manifold underneath the CALM buoy. This investigation presents the sensitivity studies on CALM buoy hose systems with improved modelling techniques on the offshore marine industry.

From this presented investigation, the following observations were made:

1. A number of deformations were observed in the hose occurs where the MBR is high. Similarly, some curvature distributions are observed from the behaviour of the submarine hoses via dynamic analysis. The models of 0° flow angle have the highest curvatures via arc length of the hose in both configurations. However, the 90° flow angle models reflected minimal curvature via the arc length of the hose. Damping is one method to minimise hose curvatures, in addition to inclusion of the hydrodynamic loads. It was also observed that the hoses subjected to cross-flow directions in the cases for 0° and greater curvatures developed on inclusion of the hydrodynamic loads.
2. In comparing the models for Lazy-S and Chinese-lantern configurations, while the curvature plot in the Lazy-S cases sag, that in the Chinese-lantern cases are hugging. Also, the curvatures in the Lazy-S appear to have higher curvatures however, this can be due to the profile length of the hose-string, and azimuthal direction of the hose. However, the comparative studies on both configurations in effective tensions show that there are higher distributions recorded in the Lazy-S case than the Chinese-lantern case, but the Chinese-lantern case has more fluctuations than the Lazy-S case. This is attributed to emanate from bending in response to waves and currents. The bending moment behaviour resulted from the twisting of the hose. For the bending moment cases, more undulations are observed in the Lazy-S cases than the Chinese-lantern cases due to the longer length of the submarine hoses and the floats attached on the submarine hose-string in the Lazy-S configuration.
3. It was also observed that the cross-flow model cases, particularly the case 0° and case 180° exhibited greater tensions in comparison to the case 90°. Thus, it can be deduced that an increase in the effective tension can be induced by increasing the hydromantic loads of the hose. In addition, the points of attachment of the hoses to the PLEM and to the manifold underneath the CALM buoy both exhibited maximum effective tensions that were of high magnitudes. Thus, the angle of inclination of design for the manifold is recommended to be at about 30°, as this manifold angle enhanced better results, but it is also subject to the manufacturer's choice, the environmental conditions, and the marine hose properties.
4. The sensitivity of the soil characteristics shows high significant influence on the hose-line behaviour and seabed resistance on the lower end of the hose, the PLEM and any attached submarine pipeline. An increase in the soil mudline shear strength, increases the seabed resistance rises steadily. This means that if submarine hoses are attached to the PLEM, there will be a noticeable dynamic lay effect. As the shear strength gradient increases, the submarine pipeline embedment will have a corresponding dynamic lay effect.
5. The sensitivity of seabed resistance on the hose-string shows that the highest soil shear stiffness of 100kN/m/m$^2$ had the least bending moment, and the least effective tension under nonlinear seabed model, which shows the influence of variation or nonlinearity due to the rate of penetration, seabed soil resistance and uplift on the seabed.
6. As the surface current velocity increases, the bend radius (curvature) decreases, the bend moment decreases and the effective tension increases. Considering the seabed currents, the following seabed current velocities were considered: 0.35 m/s, 0.45 m/s, 0.75 m/s and 0.9 m/s. For the same surface current velocity, an increase in the seabed

current velocity has a reduced effective tension and reduced bend moment. An increase in seabed current velocity gives a reduced bend radius (Curvature), increased effective tension and bend moment.

7. The surface wave is highly significant in the dynamic responses of the hose-line, the buoy stability, and the seabed resistance. The most critical wave direction is the following sea (0° flow angle) followed by the stern-quartering seas (30° and 60° flow angle). Naturally, an increase in wave height increases the submarine hoses' dynamic responses and seabed resistance. However, suggestions include further studies to investigate the approximations analytically for the moving boundary of submarine hoses and the description of the moving boundary of submarine hoses. Also, dynamical formulations are necessary to understand further the stability and dynamics behaviour of CALM buoy hoses systems, such as the hose-snaking phenomenon.
8. This study also shows a variation in the effect of current velocity from different motion characteristics due to the resonating frequency. The effect of the current velocity is relative to the motion- if translational like surge and heave, or rotational like pitch and yaw. In the heave case, the frequency profile is higher from 0.299Hz to 1.223Hz, unlike in the surge motion, where the frequency profile is 0.179Hz to 0.278Hz. This behaviour shows a relationship between first-order wave forces and the three (3) current velocities investigated. Similar findings were observed when current velocity was investigated for the motion RAOs of the CALM buoy.

## 5. Concluding Remarks

Some investigations on marine bonded hoses connected to CALM buoy have been presented on hydrodynamic characteristics, wave-current interaction, and sensitivity analysis. The models were conducted for application in shallow water and deep water conditions. The RAO values generated from ANSYS AQWA were directly coupled upon the FEM-Orcaflex model developed based on Orcaflex Line theory. This Orcaflex line theory uses the nodes along with the hoses and mooring lines but applies some discretization for the CALM buoy. This technique aids in utilising less computational time and resources. Different environmental conditions, mooring line conditions, and hose load cases were considered in developing the model. Comparisons and sensitivity of various parameters were also conducted in this study. In addition, some results of decay test were presented on the study to ascertain the buoy motion response. The investigation has also given trends and profiles for the buoy and marine hoses under wind, waves, and current.

The model highlights include: some studies on wave-current interaction, currents effects, soil strength, time response, and wave loads on marine bonded hoses are presented. Secondly, sensitivity analysis based on a coupled approach using the RAO from ANSYS AQWA inputted unto Orcaflex in the dynamic process. This concept has been applied to flexible risers, steel catenary risers (SCRs), and pipelay analysis. This proposed method saves computational resources, is cost-effective, and has high accuracy. Thirdly, the global response analysis on the effect of wave angle, soil characteristics, and current on the submarine hoses were considered under different ocean conditions. Fourthly, sensitivity from the application of DAF on the offshore submarine hoses for Lazy-S and Chinese-lantern configurations with proposed $DAF_{Hose}$ values based on the effect of hydrodynamics loads from the buoy response on the tension of the submarine hoses based on present study. Lastly, the model presents the motion scenario by analysing the bending and deflection which has an advantage in predicting the behaviour of submarine hoses.

The study shows hydrodynamic characteristics of CALM buoy hose systems under wind, waves, and current. It also indicates limits of tensile bending from different hose parameters on the marine hose-string, the hose behaviour, and the hose configuration from the sensitivity study. It discusses that these parameters influence the submarine hose configuration by providing unique curvature and tension distributions. The results of this study will also aid hose manufacturers in solving the challenge of large deformations experienced during service operations of marine bonded hoses. These findings can be used to elaborate existing standards such as OCIMF [33-36], DNVGL [132-134], ABS [135] and API [164]. Also, it presents an understanding of the issue of high curvature profiles experienced on marine hoses that lead to their failures. This study also contributes to the knowledge of buoy hydrodynamics under low/high amplitude waves. From this investigation, recommendations are made that will aid the improvement of buoy-hose performance. However, it is recommended that experiments are conducted on the marine hose systems using model tests for CALM buoy systems to improve validations on these systems. Lastly, comparing the analytical model and computational fluid dynamics (CFD) using some hydrodynamic characteristics will increase its validity, but recommended in further studies.

**Supplementary Materials:** None provided at this time.

**Author Contributions:** Conceptualization, C.V.A., F.W., J.Y.; methodology, C.V.A., F.W., J.Y.; software, C.V.A., F.W., J.Y.; validation, C.V.A., F.W., J.Y.; formal analysis, C.V.A., F.W., J.Y.; investigation, C.V.A., F.W., J.Y.; resources, C.V.A., J.Y.; data curation, C.V.A., F.W., J.Y.; writing—original draft preparation, C.V.A.; writing—review and editing, C.V.A., F.W., J.Y.; visualization, C.V.A., F.W., J.Y.; supervision, C.V.A., F.W., J.Y.; project administration, C.V.A., F.W., J.Y.; funding acquisition, C.V.A., F.W., J.Y.; All author(s) have read and agreed to the published version of the manuscript.

**Funding:** The Department of Engineering, Lancaster University, UK and EPSRC's Doctoral Training Centre (DTC), UK are highly appreciated. In addition, the funding of Overseas Scholarships by Niger Delta Development Commission (NDDC), Port harcourt, Nigeria is also appreciated and the support of Standards Organisation of Nigeria (SON) F.C.T Abuja, Nigeria. We also acknowledge National Natural Science Foundation of China (NSFC) for supporting the Projects 51922064 and 51879143, including this study. The article processing charges (APC) for this article was funded by Author 1 – C.V.A, with support from MDPI's JMSE.

**Institutional Review Board Statement:** Not applicable.

**Informed Consent Statement:** Not applicable.

**Data Availability Statement:** The raw/processed data required to reproduce these findings cannot be shared at this time, as the data also forms part of an ongoing study.

**Acknowledgments:** The authors acknowledge the technical support from Lancaster University Engineering Department staff. The authors are grateful to Abiodun K. Oyetunji of Lancaster University, for reviewing this manuscript. Lastly, the users support team of the ANSYS and Orcaflex's Orcina, UK is appreciated for technical support. The authors appreciate the feedback of the reviewers and the editors on this submission.

**Conflicts of Interest:** The authors declare no conflict of interest. The funders had no role in the design of the study; in the collection, analyses, or interpretation of data; in the writing of the manuscript, or in the decision to publish the results.

## Abbreviations

| | |
|---|---|
| $v$ | Fluid velocity |
| $\rho$ | Density of water |
| $\omega$ | Angular frequency |
| $\omega_p$ | Peak angular frequency |
| $\gamma$ | Peak enhancement factor |
| $\eta$ | The incident wave amplitude |
| $\lambda$ | Wavelength |

| | |
|---|---|
| $\theta$ | Angle to the horizontal axis |
| 3D | Three Dimensional |
| 6DoF | Six Degrees of Freedom |
| ABS | American Bureau of Shipping |
| API | America Petroleum Institute |
| BEM | Boundary Element Method |
| BM | Bending Moment |
| BVP | Boundary Value Problem |
| CALM | Catenary Anchor Leg Mooring |
| CB | Cylindrical Buoy |
| CFD | Computational Fluid Dynamics |
| CMS | Conventional Mooring Systems |
| DAF | Dynamic Amplification Factor |
| $DAF_{hose}$ | Dynamic Amplification Factor of hose |
| DNVGL | Det Norkse Veritas & Germanischer Lloyd |
| DoF | Degree of Freedom |
| fds | fully developed sea |
| FEA | Finite Element Analysis |
| FEM | Finite Element Model |
| FOS | Floating Offshore Structure |
| FPSO | Floating Production Storage and Offloading |
| FSO | Floating Storage and Offloading |
| GMPHOM | Guide to Manufacturing and Purchasing Hoses for Offshore Moorings |
| GoM | Gulf of Mexico |
| HEV | Hose End Valve |
| HOT | Higher Order Terms |
| $H_s$ | Significant wave height |
| ID | Inner Diameter |
| JONSWAP | Joint North Sea Wave Project |
| IVC | Initial Boundary Condition |
| MBC | Marine Breakaway Coupling |
| MBR | Minimum Bearing Radius |
| ML01 | Mooring Line 01 |
| ML06 | Mooring Line 06 |
| MSL | Mean Sea Level |
| OCIMF | Oil Companies International Marine Forum |
| OD | Outer Diameter |
| PCSemi | Paired Column Semisubmersible |
| PLEM | Pipeline End Manifold |
| RAO | Response Amplitude Operator |
| s | Arc length |
| $S_B$ | Mean Wetted Surface |
| SCR | Steel Catenary Riser |
| SLWR | Steel Lazy Wave Catenary Risers |
| SPM | Single Point Mooring |
| TDP | Touch Down Point |
| TDZ | Touch Down Zone |
| te-m | metric tonne-meter |
| $T_H$ | Horizontal tension force |
| $T_p$ | Peak period |
| $T_v$ | Vertical tension force |
| TTR | Top Tensioned Riser |
| $T_z$ | Zero crossing period |
| VIV | Vortex Induced Vibration |
| VLFS | Very Large Floating Structures |
| WCI | Waves-Current Interaction |

| | |
|---|---|
| WEC | Wave Energy Converters |
| $w_s$ | Submerged weight |
| WSI | Wave-Structure Interaction |
| x | Section length of the mooring line |
| z | Height above seabed |

## References


1. Amaechi, C.V. (2022). Novel design, hydrodynamics and mechanics of marine hoses in oil/gas applications. PhD Thesis. Lancaster University, Engineering Department, Lancaster, UK, 2021 (in view).
2. Amaechi, C.V. & Ye, J., (2017). A numerical modeling approach to composite risers for deep waters. In *International Conference on Composite Structures (ICCS20) Proceedings*, Paris, France; 4–7 September 2017; Società Editrice Esculapio: Bologna, Italy.
3. Amaechi, C.V.; Odijie, C.; Sotayo, A.; Wang, F.; Hou, X.; Ye, J. Recycling of Renewable Composite Materials in the Offshore Industry. Encycl. Renew. Sustain. Mater. 2019, 2, 583–613, doi:doi:10.1016/B978-0-12-803581-8.11445-6.
4. Amaechi, C.V.; Odijie, C.; Etim, O.; Ye, J. Economic Aspects of Fiber Reinforced Polymer Composite Recycling. Encycl. Renew. Sustain. Mater. 2019, 2, 377–397, doi: 10.1016/B978-0-12-803581-8.10738-6.
5. Amaechi, C.V., Ye J. Local tailored design of deep water composite risers subjected to burst, collapse and tension loads. *Ocean Engineering* 2021, https://doi.org/10.1016/j.oceaneng.2021.110196.
6. Amaechi, C.V. A review of state-of-the-art and meta-science analysis on composite risers for deep seas. *Ocean. Eng*. 2021, under review.
7. Amaechi, C.V. Development of composite risers for offshore applications with review on design and mechanics. *Ships Offshore Struct*. 2021, under review.
8. Amaechi, C.V., Chesterton C., Butler H.O., Wang F., Ye J. An Overview on Bonded Marine Hoses for sustainable fluid transfer and (un)loading operations via Floating Offshore Structures (FOS). *J. Mar. Sci. Eng*. **2021**, *9*(11), 1236; **https://doi.org/10.3390/jmse9111236**.
9. Amaechi, C.V, Chesterton C., Butler H.O., Wang F., Ye J. Review on the design and mechanics of bonded marine hoses for Catenary Anchor Leg Mooring (CALM) buoys. *Ocean Eng*. Volume 242, 15 December 2021, 110062. https://doi.org/10.1016/j.oceaneng.2021.110062
10. Ye, J.; Cai, H.; Liu, L; Zhai, Z.; Amaechi, C.V.; Wang, Y.; Wan, L.; Yang, D.; Chen, X.; Ye, J. Microscale intrinsic properties of hybrid unidirectional/woven composite laminates: Part I experimental tests. Compos. Struct. 2020, 262, 113369, doi:10.1016/j.compstruct.2020.113369.
11. Amaechi C. V., Gillett N., Odijie A. C., Hou X., and Ye J. (2019). "Composite Risers for Deep Waters Using a Numerical Modelling Approach," *Compos. Struct.*, vol. 210, no. 2019, pp. 486–499, 2019. https://doi.org/10.1016/j.compstruct.2018.11.057
12. Amaechi C. V., Gillett N., Odijie A. C., Wang F., Hou X., and Ye J. (2019). "Local and Global Design of Composite Risers on Truss SPAR Platform in Deep waters," in *Proceedings of 5th International Conference on Mechanics of Composites*, Instituto Superior de Tecnico, Lisbon, Portugal, 1–4 July 2019; no. 20005, pp. 1–3.
13. Amaechi, C.V. Numerical study on plastic deformation, plastic strains and bending of tubular pipes. Inventions 2021, under review.

14. Wang F. (2018). Effective design of submarine pipe-in-pipe using Finite Element Analysis. Ocean Eng. 2018, 153, 23–32. https://doi.org/10.1016/j.oceaneng.2018.01.095
15. Wang, F.; Han, L. Analytical behaviour of carbon steel-concrete-stainless steel double skin tube (DST) used in submarine pipeline structure. Mar. Struct. 2019, 63, 99–116. https://doi.org/10.1016/j.marstruc.2018.09.001
16. Wang, F.; Han, L.; Li, W. Analytical behavior of CFDST stub columns with external stainless steel tubes under axial compression. Thin-Walled Struct. 2018, 127, 756–768, doi:10.1016/j.tws.2018.02.021.
17. Wang, J.-T.; Wang, F.-C. Analytical behavior of built-up square concrete-filled steel tubular columns under combined preload and axial compression. Steel Compos. Struct. 2021, 38, 617–635. doi:10.12989/scs.2021.38.6.617.
18. EMSTEC (2016). EMSTEC Loading & Discharge Hoses for Offshore Moorings; EMSTEC: Rosengarten, Germany, 2016. Available at: https://denialink.eu/pdf/emstec.pdf (Accessed on: 29th September, 2021).
19. Yokohama (2016). Seaflex Yokohama Offshore Loading & Discharge Hose. The Yokohama Rubber Co. Ltd. Hiratsuka City, Japan. Available at: https://www.y-yokohama.com/global/product/mb/pdf/resource/seaflex.pdf (Accessed on 17th May 2021).
20. Amaechi, C.V., Wang, F.; Ye, J. Numerical studies on CALM buoy motion responses, and the effect of buoy geometry cum skirt dimensions with its hydrodynamic waves-current interactions. Ocean Eng. 2021, under review.
21. Amaechi, C.V., Chesterton C., Odijie C.A., Wang F., Ye J. Numerical assessment of offshore hose load response during reeling and free-hanging operations under ocean waves. *Marine Structures* 2021, under review.
22. Amaechi, C.V. Analytical cum numerical solutions on added mass and damping of a CALM buoy towards understanding the fluid-structure interaction of marine bonded hose under random waves. *Mar. Struct.* 2021, under review.
23. Amaechi, C.V.; Wang, F.; Ye, J. Understanding the fluid-structure interaction from wave diffraction forces on CALM buoys: Numerical and analytical solutions. *Ships Offshore Struct.* 2021, https://doi.org/10.1080/17445302.2021.2005361.
24. Amaechi, C.V., Wang, F.; Ye, J. Numerical Assessment on the Dynamic Behaviour of Submarine Hoses Attached to CALM Buoy Configured as Lazy-S under Water Waves. *J. Mar. Sci. Eng.* **2021**, *9*(10), 1130; **https://doi.org/10.3390/jmse9101130**.
25. Amaechi, C.V. Experimental study on motion characterization of CALM buoy hose system with CFD investigation on vortex effect. *J. Mar. Sci. Eng.*, 2021, under review.
26. Odijie, A.C., Quayle, S. & Ye, J., 2017. Wave induced stress profile on a paired column semisubmersible hull formation for column reinforcement. Engineering Structures, 143(April), pp.77–90. Available at: http://dx.doi.org/10.1016/j.engstruct.2017.04.013.
27. Odijie, A.C., Wang, F. & Ye, J., 2017. A review of floating semisubmersible hull systems: Column stabilized unit. Ocean Engineering, 144(October 2016), pp.191–202. Available at: https://doi.org/10.1016/j.oceaneng.2017.08.020.
28. Odijie, A.C. & Ye, J., 2015. Understanding Fluid-Structure Interaction for high amplitude wave loadings on a deep-draft paired column semi-submersible platform: a finite element approach. International Conference on Light Weight Design of Marine Structures, Glasgow, UK. DOI: 10.13140/RG.2.1.3259.5283
29. Odijie, A.C. & Ye, J., 2015. Effect of Vortex Induced Vibration on a Paired-Column SemiSubmersible Platform. International Journal of Structural Stability Dynamics, 15(8). doi:10.1142/s0219455415400192.
30. Amaechi, C.V. Parametric investigation on tensioner stroke analysis, recoil analysis and disconnect for the marine drilling riser of a Paired Column Semisubmersible under deep water waves. Ocean. Eng. 2021, under

review.

31. Amaechi, C.V. Dynamic analysis of tensioner model applied on global response of marine riser recoil and disconnect. Ocean. Eng. 2021, under review.
32. Amaechi, C.V. Effect of marine riser integration for characteristic motion response studies on a Paired Column Semisub-mersible in deep waters. Mar. Struct. 2021, under review.
33. Amaechi, C.V. Numerical investigation on mooring line configurations of a Paired Column Semisubmersible for its global performance in deep water condition. Ocean. Eng. 2021, under review.
34. OCIMF. Guide to Manufacturing and Purchasing Hoses for Offshore Moorings (GMPHOM); Witherby Seamanship International Ltd.: Livingstone, UK, 2009.
35. OCIMF. Guideline for the Handling, Storage, Inspection and Testing of the Hose, 2nd ed.; Witherby & Co. Ltd.: London, UK, 1995.
36. OCIMF. Single Point Mooring Maintenace and Operations Guide (SMOG); Witherby & Co. Ltd.: London, UK, 1995.
37. Amaechi, C.V. Single Point Mooring (SPM) hoses and Catenary Anchor Leg Mooring (CALM) buoys. LinkedIn Pulse. Published on 26 July 2021. Available online: https://www.linkedin.com/pulse/single-point-mooring-spm-hoses-catenary-anchor-leg-calm-amaechi (Accessed on 1 Sep-tember 2021).
38. Trelleborg. Trelleborg Oil & Gas Solutions: Oil & Gas Hoses for Enhanced Fluid Transfer Solutions; Vol. 1, page 1-30. Trelleborg Fluid Handling Solutions. Oil & Marine Hoses: Innovation and Safety for Oil & Gas Transfer Systems. Trelleborg: Clemont-Ferrand, France. 2018.
39. Bluewater Energy Services. Buoyed Up: The Future of Tanker Loading/Offloading Operations; Bluewater Energy Services: Amsterdam, The Netherlands, 2009. Available at: https://www.bluewater.com/wp-content/uploads/2013/04/CALM-Buoy-brochure-English.pdf (Accessed on: 18th July, 2021).
40. Continental. Marine Hose Brochure. 2020. Available online: https://aosoffshore.com/wp-content/uploads/2020/02/ContiTech_Marine-Brochure.pdf (Accessed on 17 February 2021).
41. Trelleborg. Surface Buoyancy. Trelleborg Marine and Infrastructure: Product Brochure. Ref.: BC-SUR-v1.3. Trelleborg Sweden, 2017. Available at: https://www.trelleborg.com/en/marine-and-infrastructure/products-solutions-and-services/marine/surface-buoyancy (Accessed on 30 September 2021).
42. Bluewater Energy Services. 2019. Oceans of knowledge. Bluewater Energy Services: Amsterdam, The Netherlands, pp. 1-20.
43. OIL. Offloading Hoses: Floating & Submarine Hoses-OIL Hoses Brochure; Offspring International Limited: Dudley, UK, 2014. Available at: https://www.offspringinternational.com/wp-content/uploads/2020/06/OIL-Offloading-Hoses-Brochure-2020-W.pdf (Accessed on 12 July 2021).
44. OIL. Mooring and Offloading Systems; Offspring International Limited: Dudley, UK, 2015. Available at: https://www.offspringinternational.com/wp-content/uploads/2015/04/OIL-SPM-Brochure-2015.pdf (Accessed on 12 July 2021).
45. Bluewater. Conventional Buoy Mooring Systems; Bluewater Energy Services: Amsterdam, The Netherlands, 2009.
46. Bluewater. Turret Buoy; Bluewater Energy Services: Amsterdam, The Netherlands, 2016.
47. ContiTech. Marine Hoses-Offshore Fluid Transfer. Contitech Oil & Gas, UK. 2017. Available online: http://www.contitech-oil-gas.com/pages/marine-hoses/marine-hoses_en.html (Accessed on 30 September 2021).
48. ContiTech. High Performance Flexible Hoses Brochure; Contitech Oil & Gas: Grimsby, UK, 2014

49. Bluewater. Bluewater Turret Buoy-Technical Description; Bluewater Energy Services: Amsterdam, The Netherlands, 2011.
50. Constantin A, Ivanov RI, Martin CI. Hamiltonian formulation for wave-current interactions in stratified rotational flows. *Archive for Rational Mechanics and Analysis* 2016;221(3):1417-1447. DOI: 10.1007/s00205-016-0990-2
51. Chen Y., Chen L., Zhang H., Gong W. (2019). Effects of wave-current interaction on the Pearl River Estuary during Typhoon Hato. Estuarine, Coastal and Shelf Science, Volume 228, 15 November 2019, 106364 https://doi.org/10.1016/j.ecss.2019.106364
52. Hegermiller C.A., Warner J.C., Olabarrieta M., and Sherwood C.R. (2019). Wave–Current Interaction between Hurricane Matthew Wave Fields and the Gulf Stream. *Journal of Physical Oceanography*, Vol. 49, Issue 11.Pages 2883-2900. https://doi.org/10.1175/JPO-D-19-0124.1
53. Jia, L., Ren, J., Nie, D. et al. Wave-current bottom shear stresses and sediment re-suspension in the mouth bar of the Modaomen Estuary during the dry season. Acta Oceanol. Sin. 33, 107–115 (2014). https://doi.org/10.1007/s13131-014-0510-x
54. Beya I., Buckham B., Robertson B. (2021). Impact of tidal currents and model fidelity on wave energy resource assessments. Renewable Energy. Volume 176, October 2021, Pages 50-66. https://doi.org/10.1016/j.renene.2021.05.039
55. Odijie, A.C., 2016. Design of paired column semisubmersible hull. PhD Thesis. Engineering Department, Lancaster University, Lancaster, UK. Available at: https://eprints.lancs.ac.uk/id/eprint/86961/1/2016AgbomeriePhD.pdf Accessed on: 12th Feb., 2020.
56. Mohamed H.A.M.A (2011). Hydrodynamic loading and responses of semisubmersibles. PhD Thesis. School of Marine Science and Technology, Newcastle University, Newcastle upon Tyne, UK. Available at: https://theses.ncl.ac.uk/jspui/bitstream/10443/1285/1/Hassan%20Mohamed%2011.pdf (Accessed on: 6th October, 2021).
57. Chen L, Basu B. Fatigue load estimation of a spar-type floating offshore wind turbine considering wave-current interactions. *Int J Fatigue*. 2018;116:421-428. https://doi.org/10.1016/j.ijfatigue.2018.06.002
58. de Jesus Henriques TA, Tedds SC, Botsari A, Najafian G, et al. The effects of wave–current interaction on the performance of a model horizontal axis-tidal turbine. Int J Mar Energy. 2014;8:17-35 https://doi.org/10.1016/j.ijome.2014.10.002
59. Hirdaris, S.; Bai, W.; Dessi, D.; Ergin, A.; Gu, X.; Hermundstad, O.; Huijsmans, R.; Iijima, K.; Nielsen, U.; Parunov, J.; et al. Loads for use in the design of ships and offshore structures. Ocean Eng. 2014, 78, 131–174, doi:10.1016/j.oceaneng.2013.09.012.
60. Bai, Y.; Bai, Q. Subsea Pipelines and Risers, 1st ed.; Elsevier: Oxford, UK, 2005.
61. Bai, Y.; Bai, Q. Subsea Engineering Handbook; Elsevier: Oxford, UK, 2010.
62. Wichers, I.J. Guide to Single Point Moorings; WMooring Inc: Houston, TX, USA, 2013.
63. Berteaux, H.O. Buoy Engineering; John Wiley and Sons: New York, NY, USA, 1976.
64. Berteaux, H.O.; Goldsmith, R.A.; Schott I.I.I., W.E. Heave and Roll Response of Free Floating Bodies of Cylindrical Shape. Report WHOI-77-12. Woods Hole Oceanographic Institution; Massachusetts, MA, USA, 1977. Available at: https://apps.dtic.mil/sti/pdfs/ADA038215.pdf (Accessed on: 15th August 2021).
65. Wilson, J.F. Dynamics of Offshore Structures, 2nd ed.; John Wiley and Sons: New Jersey, USA, 2003.
66. Sorensen, R.M. Basic Coastal Engineering, 3rd ed.; Springer: New York, NY, USA, 2006.

67. Sorensen, R.M. Basic Wave Mechanics: For Coastal and Ocean Engineers; John Wiley and Sons: London, UK. 1993
68. Havelock, T.H., 1940. The Pressure of Water Waves upon a Fixed Obstacle. *Proceedings of the Royal Society of London. Series A , Mathematical and Physical Sciences*, 175(963), pp.409–421. https://doi.org/10.1098/rspa.1940.0066
69. MacCamy, R.C. & Fuchs, R.A., 1954. *Wave forces on piles: a diffraction theory*, Report BEB-TM-69, Beach Erosion Board, Department of Army, USA. Washington D.C., USA. Pages 1-17. Available at: https://erdc-library.erdc.dren.mil/jspui/bitstream/11681/3444/1/BEB-TM-69.pdf (Accessed on: 8th September, 2021).
70. Chakrabarti S.K. (1972). Nonlinear wave forces on vertical cylinder. Journal of Hydraulics division, Proceedings of the American Society of Civil Engineers, Vol. 102, No. HY11, November 1972.
71. Chakrabarti, S.K., 1975. Second-Order Wave Force on Large Vertical Cylinder. Journal of the Waterways, Harbors and Coastal Engineering Division, 101(3), pp.311–317.
72. Rahman, M. Non-linear wave loads on large circular cylinders: a perturbation technique. Adv. Water Resour. 1981, 4, 9–19, doi:10.1016/0309-1708(81)90003-8.
73. Rahman, M. Second order wave interaction with large structures. In Wave Phenomena: Modern Theory and Applications; Rogers, T.B.M.C., Ed.; Elsevier B.V: North Holland, The Netherlands, 1984; pp. 49–69. North-Holland Mathematics Studies, Volume 97, 1984, Pages 49-69. https://doi.org/10.1016/S0304-0208(08)71254-4
74. Newman J.N. 1996. The second-order wave force on a vertical cylinder. Journal of Fluid Mechanics, Volume 320, pp. 417 - 443 https://doi.org/10.1017/S0022112096007598
75. Ghalayini & Williams 1991. Nonlinear wave forces on vertical cylinder arrays. Journal of Fluids and Structures. Volume 5, Issue 1, January 1991, Pages 1-32. https://doi.org/10.1016/0889-9746(91)80009-3
76. Zhang S., Chen C., Zhang Q.-X., Zhang D.-M., Zhang F. (2015). Wave Loads Computation for Offshore Floating Hose Based on Partially Immersed Cylinder Model of Improved Morison Formula. *The Open Petroleum Engineering Journal*, 2015, 8, 130-137. Publisher Id TOPEJ-8-130, DOI: 10.2174/1874834101508010130
77. Liu B., Fu D., Zhang Y., Chen X. (2020). Experimental and numerical study on the wave force calculation of a partially immersed horizontal cylindrical float. *International Journal of Naval Architecture and Ocean Engineering.* Volume 12, 2020, Pages 733-742. https://doi.org/10.1016/j.ijnaoe.2020.08.002
78. Morison, J.R., Johnson J.W., Schaaf S.A. 1950. The Force Exerted by Surface Waves on Piles. *Petroleum Transactions*, Paper Number: SPE-950149-G. *AIME*, 189. *J Pet Technol* 2 (05). pp.149–154. https://doi.org/10.2118/950149-G
79. Brebbia, C.A. & Walker, S., 2013. Dynamic Analysis of Offshore Structures, 2013 Reprint of 1979 Ed.; London, UK: Newnes-Butterworth & Co. Publishers Ltd.
80. Sarpkaya, T., 2014. Wave forces on offshore structures 1st ed., New York, USA: Cambridge University Press.
81. Chandrasekaran, S., 2015. Dynamic Analysis and Design of Offshore Structures 1st Ed., India: Springer.
82. Chandrasekaran, S., Jain, A.K. & Chandak, N.R., 2007. Response Behavior of Triangular Tension Leg Platforms under Regular Waves Using Stokes Nonlinear Wave Theory. Journal of Waterway, Port, Coastal, and Ocean Engineering, 133(3), pp.230–237.
83. Chakrabarti S. K., Handbook of Offshore Engineering - Volume 1. Oxford, UK: Elsevier, 2005.
84. Chakrabarti S. K., Handbook of Offshore Engineering - Vol. 2, vol. II. Oxford, UK: Elsevier, 2006.
85. Cozijn, J.L.; Bunnik, T.H.J. Coupled Mooring Analysis for a Deep Water CALM Buoy. In Proceedings of the 23rd International Conference on Offshore Mechanics and Arctic Engineering (OMAE), Vancouver, BC, 2004; OMAE2004-51370; Volume 1, Parts A and B. Vancouver, British Columbia, Canada. June 20–25, 2004. pp. 663-

673. ASME. The American Society of Mechanical Engineers: New York, NY, USA, 2004 pp. 1–11. https://doi.org/10.1115/OMAE2004-51370

86. Cozijn, H., Uittenbogaard, R. & Brake, E. Ter, 2005. Heave , Roll and Pitch Damping of a Deepwater CALM Buoy with a Skirt. In *International Society of Offshore and Polar Engineering Conference* (ISOPE) *Proceedings*. *Seoul, Korea, 19–24 June 2005*; ISOPE: Cupertino, CA, USA; Volume 8, pp. 388–395. Available at: https://www.researchgate.net/publication/267364857_Heave_Roll_and_Pitch_Damping_of_a_Deepwater_CALM_Buoy_with_a_Skirt (Accessed on: 11 September, 2021).
87. Rahman, M. & Chakravartty, I.. C.., 1981. Hydrodynamic Loading Calculations for Offshore Structures. SIAM Journal on Applied Mathematics, 41(3), pp.445–458. https://doi.org/10.1137/0141037
88. Raman H.  & Venkatanarasaiah (1976). Forces due to nonlinear wavs on vertical cylinders. Journal of the Waterways Harbors and Coastal Engineering division, Proceedings of the American Society of Civil Engineers, Vol. 102, No. WW3, August 1976. https://doi.org/10.1061/AWHCAR.0000331
89. Bhatta, D.D. & Rahman, M., 2003. On scattering and radiation problem for a cylinder in water of finite depth. International Journal of Engineering Science, 41, pp.931–967. DOI: 10.1016/S0020-7225(02)00381-6
90. Lighthill, J., 1979. Waves and hydrodynamic loading. In Proc. 2nd. Int. Conf. Behavior of Offshore Structures (BOSS '79). London, pp. 1–40.
91. Lighthill, J., 1986. Fundamentals concerning wave loading on offshore structures. J . Fluid Mechanics, 173(1), pp.667–681. https://doi.org/10.1017/S0022112086001313
92. Brown, M.J.; Elliott, L. Two-dimensional dynamic analysis of a floating hose string. Appl. Ocean Res. 1988, 10, 20–34. https://doi.org/10.1016/S0141-1187(88)80021-X.
93. Brown, M.J. Mathematical Model of a Marine Hose-String at a Buoy—Part 1—Static Problem. In Offshore and Coastal Modelling; Dyke, P., Moscardini, A.O., Robson, E.H., Eds.; Springer: London, UK, 1985; pp. 251–277. https://doi.org/10.1007/978-1-4684-8001-6_14.
94. Brown, M.J. Mathematical Model of a Marine Hose-String at a Buoy—Part 2—Dynamic Problem. In Offshore and Coastal Modelling; Dyke, P., Moscardini, A.O., Robson, E.H., Eds.; Springer: London, UK, 1985; pp. 279–301. https://doi.org/10.1007/978-1-4684-8001-6_13.
95. Huang, T.S. & Leonard, J.W., 1989. Lateral Stability of a flexible submarine hoseline, Port Hueneme, California, USA. Available at: https://apps.dtic.mil/sti/pdfs/ADA219251.pdf  (Accessed on: 8th September, 2021).
96. Bree, J.; Halliwell, A.R.; O'Donoghue, T. Snaking of floating marine oil hose attached to SPM buoy. J. Eng. Mech. 1989, 115, 2, 265–284. https://doi.org/10.1061/(ASCE)0733-9399(1989)115:2(265)
97. O'Donoghue, T.;Halliwell, A, R. Floating Hose-Strings Attached to a CALM Buoy. In Proceedings of the Offshore Technology Conference, Houston, Texas, 2–5 May 1988; OTC 5717; pp. 313–320. https://doi.org/10.4043/5717-MS
98. O'Donoghue, T.; Halliwell, A.R. Vertical bending moments and axial forces in a floating marine hose-string. Eng. Struct. 1990, 12, 4, 124–133. https://doi.org/10.1016/0141-0296(90)90018-N
99. O'Donoghue, T. The Dynamic Behaviour of a Surface Hose Attached to a CALM Buoy. Ph.D. Thesis. Department of Offshore Engineering, Heriot-Watt University, Edinburgh, UK. Available online: https://www.ros.hw.ac.uk/bitstream/10399/1045/1/O%27DonoghueT_0587_epsBL.pdf (Accessed on: 1 September 2021).
100. Amaechi, C.V., Wang F., Ye J. Mathematical Modelling of Bonded Marine Hoses for Single Point Mooring (SPM) Systems, with Catenary Anchor Leg Mooring (CALM) Buoy application- A Review. *J. Mar. Sci. Eng*. 2021, 9(11), 1179; https://doi.org/10.3390/jmse9111179.

101. Edward, C.; Dev, A.K. Assessment of CALM Buoys Motion Response and Dominant OPB/IPB Inducing Parameters on Fatigue Failure of Offshore Mooring Chains. In *Practical Design of Ships and Other Floating Structures. PRADS 2019. Lecture Notes in Civil Engineering*, Okada, T., Suzuki, K., Kawamura, Y, Eds.; Springer: Singapore, 2021; Volume 64, doi.org/10.1007/978-981-15-4672-3_35.
102. Bridgestone, J., 1976. Study of causes of kinking in floating hoses at Petrobras/Tefran terminal. Report No. 6YMT-0011, Japan.
103. Dennis Denney (2006). Chain Failure by Bending on Deepwater Mooring Systems. J Pet Technol 58 (02): 72–73. Paper Number: SPE-0206-0072-JPT https://doi.org/10.2118/0206-0072-JPT
104. Brady, I., Williams, S. & Golby, P., 1974. A study of the Forces Acting on Hoses at a Monobuoy Due to Environmental Conditions. In *Offshore Technology Conference Proceeding -OTC 2136*. Dallas, Texas, USA: OnePetro, May 5–7, 1974. pp. 1–10. https://doi.org/10.4043/2136-MS
105. Ryu, S.; Duggal, A.S.; Heyl, C.N.; Liu, Y. Prediction of Deepwater Oil Offloading Buoy Response and Experimental Validation. Int. J. Offshore Polar Eng. 2006, 16, 3, 1–7. Available at: https://www.sofec.com/wp-content/uploads/white_papers/2006-ISOPE-Prediction-of-DW-Oil-Offloading-Buoy-Response.pdf (Accessed on: 11 September 2021).
106. Duggal, A. & Ryu, S., 2005. The dynamics of deepwater offloading buoys. In: *WIT Transactions on The Built Environment*. Paper FSI05026FU, WIT Press, Singapore. Available at: https://www.witpress.com/Secure/elibrary/papers/FSI05/FSI05026FU.pdf (Accessed on: 6th July, 2021).
107. Le Cunff, C., Ryu, S, Duggal, AS., Ricbourg C., Heurtier, J, Heyl C., Liu Y., Beauclair O., 2007. Derivation of CALM Buoy coupled motion RAOs in Frequency Domain and Experimental Validation. In *International Society of Offshore and Polar Engineering Conference Proceedings*. Lisbon, Portugal: ISOPE, pp. 1–8. Available at: https://www.sofec.com/wp-content/uploads/white_papers/2007-ISOPE-Derivation-of-CALM-Buoy-Coupled-Motion-RAOs-in-Frequency-Domain.pdf (Accessed on: 11 September, 2021).
108. Le Cunff, C., Ryu, S, Heurtier, J, & Duggal, AS. "Frequency-Domain Calculations of Moored Vessel Motion Including Low Frequency Effect." *Proceedings of the ASME 2008 27th International Conference on Offshore Mechanics and Arctic Engineering. Volume 1: Offshore Technology*. Estoril, Portugal. June 15–20, 2008. pp. 689-696. ASME. https://doi.org/10.1115/OMAE2008-57632
109. Wang, F.-C.; Wang, J.; Tang, K. A finite element based study on lowering operation of subsea massive structure. *China Ocean Eng.* **2017**, *31*, 646–652, doi:10.1007/s13344-017-0074-6.
110. Lenci, S.; Callegari, M. Simple analytical models for the J-lay problem. *Acta Mech.* **2005**, *39*, 23–39. https://doi.org/10.1007/s00707-005-0239-x
111. Li, FZ, & Low, YM. (2010). "Sensitivity Study of Critical Parameters Influencing the Uncertainty of Fatigue Damage in Steel Catenary Risers." Proceedings of the ASME 2010 29th International Conference on Ocean, Offshore and Arctic Engineering. 29th International Conference on Ocean, Offshore and Arctic Engineering: Volume 2. Shanghai, China. June 6–11, 2010. pp. 31-39. ASME. https://doi.org/10.1115/OMAE2010-20045
112. Senra S. F., Jacob B. P., Torres F.L., Lúcia A., and Mourelle M. M. (2002). "Sensitivity Studies On the Fatigue Behavior of Steel Catenary Risers." Paper presented at The Twelfth International Offshore and Polar Engineering Conference, Kitakyushu, Japan, May 2002. Paper Number: ISOPE-I-02-162. Available at: https://onepetro.org/ISOPEIOPEC/proceedings-abstract/ISOPE02/All-ISOPE02/ISOPE-I-02-162/8754
113. Pecher, A.; Foglia, A.; Kofoed, J.P. Comparison and sensitivity investigations of a CALM and SALM type mooring system for wave energy converters. J. Mar. Scie. Eng. 2014, 2, 93–122, doi:10.3390/jmse2010093.
114. Sun, H, & Wang, D. "Sensitivity Analysis of Buoyancy Modules Parameters of Lazy-Wave Flexible Riser." Proceedings of the ASME 2013 32nd International Conference on Ocean, Offshore and Arctic Engineering.

Volume 4A: Pipeline and Riser Technology. Nantes, France. June 9–14, 2013. V04AT04A037. ASME. https://doi.org/10.1115/OMAE2013-10498

115. Amaechi, C.V.; Ye, J.; Hou, X.; Wang, F.-C. Sensitivity Studies on Offshore Submarine Hoses on CALM Buoy with Comparisons for Chinese-Lantern and Lazy-S Configuration OMAE2019-96755. In Proceedings of the 38th International Conference on Ocean, Offshore and Arctic Engineering, Glasgow, Scotland, 9–14 June 2019; American Society of Mechanical Engineers: New York, NY, USA, 2019.
116. Bidgoli S.I., Shahriari S., Edalat P. (2017). Sensitive Analysis of Different Types of Deep Water Risers to Conventional Mooring Systems. International Journal of Coastal & Offshore Engineering, JCOE No. 5/ Winter 2017, pp. 45-55. Available at: http://ijcoe.org/article-1-90-en.pdf (Accessed on 20th July, 2021).
117. Axelsson, G, & Skjerve, H. (2014). "Flexible Riser Carcass Collapse Analyses: Sensitivity on Radial Gaps and Bending." Proceedings of the ASME 2014 33rd International Conference on Ocean, Offshore and Arctic Engineering. Volume 6A: Pipeline and Riser Technology. San Francisco, California, USA. June 8–13, 2014. V06AT04A059. ASME. https://doi.org/10.1115/OMAE2014-23922
118. Tang L, Huang Z, Zhu X, Zhou Y, Li B. Investigation of the mechanical response of a deep-water drilling riser to ocean currents and waves. Advances in Mechanical Engineering, Vol. 11 (1), pp. 1-11. January 2019. DOI: https://doi.org/10.1177/1687814018818334
119. Zhang J., Guo H., Tang Y., Li Y. (2020). Effect of Top Tension on Vortex-Induced Vibration of Deep-Sea Risers. Journal of Marine Science and Engineering JMSE, Vol. 8, 121; DOI: 10.3390/jmse8020121
120. Li, FZ, & Low, YM. (2010). "Sensitivity Study of Critical Parameters Influencing the Uncertainty of Fatigue Damage in Steel Catenary Risers." Proceedings of the ASME 2010 29th International Conference on Ocean, Offshore and Arctic Engineering. 29th International Conference on Ocean, Offshore and Arctic Engineering: Volume 2. Shanghai, China. June 6–11, 2010. pp. 31-39. ASME. https://doi.org/10.1115/OMAE2010-20045
121. Yang, H.Z., Li, H.-J. (2011). Sensitivity Analysis of Fatigue Life Prediction for Deepwater Steel Lazy Wave Catenary Risers. Science China Technological Sciences, 54(7):1881-1887. DOI: 10.1007/s11431-011-4424-y.
122. Wang, K., Ji, C., Xue, H. et al. (2017). Fatigue sensitivity analysis of steel catenary riser near touchdown point. J. Shanghai Jiaotong Univ. (Sci.) 22, 570–576. https://doi.org/10.1007/s12204-017-1876-7
123. Quéau L.M, Kimiaei M., Randolph M.F. (2015). Sensitivity studies of SCR fatigue damage in the touchdown zone using an efficient simplified framework for stress range evaluation. Ocean Engineering, Vol. 96, Pages 295-311 https://doi.org/10.1016/j.oceaneng.2014.12.038
124. Yoo K.K. & Joo Y. (2017). Sensitivity Study on SCR Design for Spread-Moored FPSO in West Africa. Journal of Ocean Eng. Technol. 2017; 31(2): 111-120. DOI: https://doi.org/10.5574/KSOE.2017.31.2.111
125. ANSYS, 2017. *ANSYS Aqwa Theory Manual, Release 18.2*, Canonsburg, Pennsylvania, USA: ANSYS Inc.
126. ANSYS, 2017. *ANSYS Aqwa User's Manual, Release 18.2*, Canonsburg, Pennsylvania, USA: ANSYS Inc.
127. Orcina, 2014. OrcaFlex Manual, Version 9.8a, Ulverton, Cumbria, UK: Orcina Ltd.
128. Orcina, 2021. Orcaflex Help Manual, Version 11.0f. Available at: https://www.orcina.com/SoftwareProducts/OrcaFlex/Documentation/index.php. (Accessed on 20th July, 2021).
129. Orcina, 2019. Orcaflex Help Manual - Line with floats: Added mass coefficients. Available at: https://www.orcina.com/webhelp/OrcaFlex/Content/html/Linewithfloats,Addedmasscoefficients.htm (Accessed on 20th July, 2021).
130. Orcina, 2020. Orcaflex Documentation, Version 11.0f. Available at: https://www.orcina.com/webhelp/OrcaFlex/Default.htm. (Accessed on 16th February, 2020).
131. Ruan, W.; Shi, J.; Sun, B.; Qi, K. Study on fatigue damage optimization mechanism of deepwater lazy wave risers based on multiple waveform serial arrangement. Ocean. Eng. 2021, 228, doi.org/10.1016/j.oceaneng.2021.108926.

132. DNVGL. *DNVGL-RP-F205 Global Performance Analysis of Deepwater Floating Structures*; Det Norske Veritas & Germanischer Lloyd: Oslo, Norway, 2017.
133. DNVGL. *DNVGL-RP-N103 Modelling and Analysis of Marine Operations*; Det Norske Veritas & Germanischer Lloyd: Oslo, Norway, 2017.
134. DNVGL. *DNVGL-OS-E403 Offshore Loading Buoys*; Det Norske Veritas & Germanischer Lloyd: Oslo, Norway, 2015.
135. ABS. *Rules For Building And Classing—Single Point Moorings*; American Bureau of Shipping: New York, NY, USA, 2017; Volume 2017.
136. Hasselmann, K.; Barnett, T.P.; Bouws, E.; Carlson, H.; Cartwright, D.E.; Enke, K.; Ewing, J.A.; Gienapp, H.; Hasselmann, D.E.; Kruseman, P.; Meerburg, A.; Müller, P.; Olbers, D.J.; Richter, K.; Sell, W.; Walden, H. Measurements of wind-wave growth and swell decay during the Joint North Sea Wave Project (JONSWAP). *Ergänzungsheft zur Dtsch. Hydrogr. Z. -Hydraulic Engineering Reports; Ergänzungsheft 8-12; Reihe Vol. A8⁰, Issue 12,* **1973**, *12*. pp. 1-90. Publisher: Deutches Hydrographisches Institut., Hamburg, Germany. Available at: http://resolver.tudelft.nl/uuid:f204e188-13b9-49d8-a6dc-4fb7c20562fc (Accessed on: 4th March, 2021).
137. Chibueze, N.O.; Ossia, C.V.; Okoli, J.U. On the Fatigue of Steel Catenary Risers. Stroj. Vestn.–J. Mech. Eng. 2016, 62, 751–756, doi:10.5545/sv-jme.2015.3060.
138. Vyzikas, T. (2014). Application of Numerical Models and Codes. A Best Practice Report prepared as part of the MERIFIC Project – Marine Energy in Far Peripheral and Island Communities (MERIFIC), University of Plymouth, Plymouth, p. 56-60.
139. Chakrabarti, S.K. Technical Note: On the formulation of Jonswap spectrum. *Appl. Ocean Res.* **1984**, *6*, 3, 175–176. https://doi.org/10.1016/0141-1187(84)90008-7
140. Isherwood, R.M. Technical Note: A revised parameterisation of the Jonswap spectrum. *Appl. Ocean Res.* **1987**, *9*, 1, 47–50. https://doi.org/10.1016/0141-1187(87)90030-7
141. Pierson, W.J.; Moskowitz, L. A proposed spectral form for fully developed wind seas based on the similarity theory of S. A. Kitaigorodskii. *J. Geophys. Res. Space Phys.* **1964**, *69*, 5181–5190, doi:10.1029/jz069i024p05181.
142. Sparks, C.P. *Fundamentals of Marine Riser Mechanics: Basic Principles and Simplified Analyses*, 2nd ed.; PennWell Books: Tulsa, USA, 2018.
143. Dareing, D.W. *Mechanics of Drillstrings and Marine Risers*, 1st ed.; ASME Press: New York, USA, 2012; doi:10.1115/1.859995.
144. Irvine, H.M. *Cable Structures*; MIT Press: Cambridge, MA, USA, 1981.
145. Fergestad, D. and Løtveit, S.A. Handbook on Design and Operation of Flexible Pipes; MARINTEK/NTNU/4Subsea, 3rd ed.; Sintef: Trondheim, Norway, 2017. ISBN 978-82-7174-285-0. Available online: https://www.4subsea.com/wp-content/uploads/2017/07/Handbook-2017_Flexible-pipes_4Subsea-SINTEF-NTNU_lo-res.pdf (accessed on 25 August 2021).
146. Amaechi, C.V.; Wang, F.; Xiaonan, H.; Ye, J. (2019). Strength of submarine hoses in Chinese-lantern configuration from hydrodynamic loads on CALM buoy. Ocean. Eng. 2019, 171, 2019, 429–442, doi:10.1016/j.oceaneng.2018.11.010.
147. Roveri, F.E.; Volnei, S.; Sagrilo, L.; Cicilia, F.B. A Case Study on the Evaluation of Floating Hose Forces in a C.A.L.M. System. In Proceedings of the 12th International Offshore and Polar Engineering Conference, Kitakyushu, Japan, 26–31 May 2002; International Society of Offshore and Polar Engineers (ISOPE): Cupertino, CA, USA; Volume 3, pp. 190–197
148. Berhault, C.; Guerin, P.; le Buhan, P.; Heurtier, J.M. Investigations on Hydrodynamic and Mechanical Coupling Effects for Deepwater Offloading Buoy. In Proceedings of the 14th International Offshore and Polar Engineering Conference, Toulon, France, 23–28 May 2004; International Society of Offshore and Polar Engineers

(ISOPE): Cupertino, CA, USA; Volume 1, pp. 374–379. Available at: https://onepetro.org/ISOPEIOPEC/proceedings-abstract/ISOPE04/All-ISOPE04/ISOPE-I-04-363/10313 (Accessed on: 11 September 2021).

149. Williams, N.A.; McDougal, W.G. Experimental Validation Of A New Shallow Water Calm Buoy Design. In Proceedings of the 32nd International Conference on Ocean, Offshore and Arctic Engineering, Volume 1: Offshore Technology. Nantes, France, 9–14 June 2013; OMAE2013-11392; V001T01A070. ASME. The American Society of Mechanical Engineers: New York, NY, USA, 2013; pp. 1–6. DOI: 10.1115/OMAE2013-11392

150. Salem, G.; Ryu, S.; Duggal, A.S.; Raju; Datla, V. Linearization of Quadratic Drag to Estimate CALM Buoy Pitch Motion in Frequency-Domain and Experimental validation. J. Offshore Mech. Arct. Eng. 2012, 134, 3–8. https://doi.org/10.1115/1.4003645

151. Wang, F.; Chen, J.; Gao, S.; Tang, K.; Meng, X. Development and sea trial of real-time offshore pipeline installation monitoring system. *Ocean Eng.* **2017**, *146*, 468–476, doi:10.1016/j.oceaneng.2017.09.016.

152. Barltrop, N.D.P.; Adams, A.J. *Dynamics of Fixed Marine Structures*, 3rd ed.; Butterworth Heinemann: Oxford, UK, 1991.

153. Barltrop, N.D.P. *Floating Structures: A Guide for Design and Analysis-Volume 1*; Oilfield Publications Limited (OPL): Herefordshire, UK, 1998.

154. Chen L. and Basu B. (2018). Wave-current interaction effects on structural responses of floating offshore wind turbines. *Wind Energy*, Vol 22; pp. 327-339. DOI: 10.1002/we.2288.

155. Newman J.N. 1994. Wave effects on deformable bodies. Applied Ocean Research. Volume 16, Issue 1, 1994, Pages 47-59. https://doi.org/10.1016/0141-1187(94)90013-2

156. Newman J.N. 1979. Absorption of wave energy by elongated bodies. Applied Ocean Research. Volume 1, Issue 4, October 1979, Pages 189-196 https://doi.org/10.1016/0141-1187(79)90026-9

157. Newman, J.N. & Lee, C.-H., 2002. Boundary-Element Methods in Offshore Structure Analysis. *Journal of Offshore Mechanics and Arctic Engineering*, 124(May 2002), pp.81–89. https://doi.org/10.1115/1.1464561

158. Brebbia, C.A. & Dominguez, J., 1977. Boundary element methods for potential problems. Applied Mathematical Modelling. Vol. 1 (7), pp.372-378, 1977. https://doi.org/10.1016/0307-904X(77)90046-4.

159. Amaechi, C.V.; Chesterton C.; Butler H.O.; Odijie C.A.; Gu Z.; Wang, F.; Hou X.; Ye, J. (2021). Finite element modelling on the mechanical behaviour of Marine Bonded Composite Hose (MBCH) under burst and collapse. *J. Mar. Sci. Eng. 2021, 9,* under review.

160. Amaechi C.V. (2022). Experiment and finite element modelling on the load response of offshore bonded loading hoses during reeling operation, normal operation and non-operation conditions. *Ocean Eng. 2021,* under review.

161. Chesterton, C., 2020. A Global and Local Analysis of Offshore Composite Material Reeling Pipeline Hose, with FPSO Mounted Reel Drum. BEng Dissertation. Engineering Department, Lancaster University, Lancaster, UK.

162. Butler, H.O, 2021. An analysis of the failure of Composite Flexible Risers. BEng Dissertation. Engineering Department, Lancaster University, Lancaster, UK.

163. Gillett, N., 2018. Design and Development of a Novel Deepwater Composite Riser. BEng Dissertation. Engineering Department, Lancaster University, Lancaster, UK.

164. API (2017). Specification for bonded flexible pipe. 3rd Edition. American Petroleum Institute, Texas, USA.